The lymph node stromal laminin α5 shapes alloimmunity

Lushen Li,[1,2] Marina W. Shirkey,[1,2] Tianshu Zhang,[1,2] Yanbao Xiong,[1,2] Wenji Piao,[1,2] Vikas Saxena,[1,2] Christina Paluskievicz,[1,2] Young Lee,[1,2] Nicholas Toney,[1] Benjamin M. Cerel,[1,3] Qinshan Li,[1] Thomas Simon,[1] Kyle D. Smith,[4] Keli L. Hippen,[4] Bruce R. Blazar,[4] Reza Abdi,[5] and Jonathan S. Bromberg[1,2]

[1]Department of Surgery, and [2]Center for Vascular and Inflammatory Diseases, University of Maryland School of Medicine, Baltimore, Maryland, USA. [3]Graduate Medical Sciences, Boston University School of Medicine, Boston, Massachusetts, USA. [4]Division of Blood and Marrow Transplantation, Department of Pediatrics, University of Minnesota Cancer Center, Minneapolis, Minnesota, USA. [5]Transplantation Research Center, Renal Division, Brigham and Women's Hospital, Harvard Medical School, Boston, Massachusetts, USA.

Lymph node stromal cells (LNSCs) regulate immunity through constructing lymphocyte niches. LNSC-produced laminin α5 (Lama5) regulates CD4⁺ T cells but the underlying mechanisms of its functions are poorly understood. Here we show that depleting Lama5 in LNSCs resulted in decreased Lama5 protein in the LN cortical ridge (CR) and around high endothelial venules (HEVs). Lama5 depletion affected LN structure with increased HEVs, upregulated chemokines, and cell adhesion molecules, and led to greater numbers of Tregs in the T cell zone. Mouse and human T cell transendothelial migration and T cell entry into LNs were suppressed by Lama5 through the receptors α6 integrin and α-dystroglycan. During immune responses and allograft transplantation, depleting Lama5 promoted antigen-specific CD4⁺ T cell entry into the CR through HEVs, suppressed T cell activation, and altered T cell differentiation to suppressive regulatory phenotypes. Enhanced allograft acceptance resulted from depleting Lama5 or blockade of T cell Lama5 receptors. Lama5 and Lama4/Lama5 ratios in allografts were associated with the rejection severity. Overall, our results demonstrated that stromal Lama5 regulated immune responses through altering LN structures and T cell behaviors. This study delineated a stromal Lama5–T cell receptor axis that can be targeted for immune tolerance modulation.

Introduction

The lymph node (LN) is the central hub that exchanges antigen-presenting cells and immune cells with peripheral tissues or blood, permitting T cells to encounter cognate antigens and orchestrating T lymphocyte immune responses (1, 2). LN architecture is primarily constructed by a group of nonhematopoietic stromal cells, which constitute approximately 1% of LN cellularity and establish specialized niches (3, 4). The LN stromal cell (LNSC) framework directs immune cell trafficking within designated compartments, which dictate leukocyte functions (5, 6). The LN 3-dimensional structure is compartmentalized by LNSCs and identified as (i) the superficial cortex constituted by follicles and interfollicular cortex; (ii) the paracortex constituted by deep cortical units; and (iii) the medulla constituted by medullary cords and medullary sinuses (7). The cortical ridge (CR) in the paracortex is the region where T lymphocytes enter from the blood and initially encounter antigen-presenting cells (8). High endothelial venules (HEVs) and lymphatic vessels cross these compartments and are crucial tunnels, exchanging cells and antigens between the LNs and other organs and tissues (9).

Based on expression of the glycoprotein podoplanin (gp38) and the adhesion molecule CD31 (PECAM-1), LNSCs are mainly classified as fibroblast reticular cells (FRCs, $CD45^-CD31^-gp38^+$), blood endothelial cells (BECs, $CD45^-CD31^+gp38^-$), and lymphatic endothelial cells (LECs, $CD45^-CD31^+gp38^+$) (10). FRCs provide a structural scaffold by producing extracellular matrix proteins such as laminins, ER-TR7, and collagen (2, 11). FRCs ensheath a conduit network that bridges the subcapsular sinus and cortex, enabling small molecules to be delivered into the LN paracortex (12–14). FRCs also produce an array of cytokines or chemokines, including IL-7, IL-15, IL-33, CXCL2, CXCL9, CXCL10, CXCL12, CXCL13, CCL19, and CCL21 (15, 16) and adhesion molecules, including I-CAM-1 and VCAM-1 (11, 17, 18), which are responsible for immune cell migration, survival, and activation (19). FRCs express peripheral tissue antigens such as pre-proinsulin 2, Gad67, MHC I, and MHC II to restrict self-reactive T cells, thereby preventing autoimmune disease (20–22). These observations highlight the profound importance of LNSCs, particularly FRCs, for the LN and T cell responses.

Laminin α4 (Lama4) and α5 (Lama5) are primary extracellular matrix components expressed on basement membranes (13, 17, 23) and are expressed by LNSC subsets including FRCs, BECs, and LECs (22). Rodda et al. identified 9 peripheral LN nonendothelial stromal cell clusters using droplet-based single-cell RNA sequencing, defining distinct LNSCs that likely support niche-restricted immune functions and provide evidence that many LNSCs are in an activated state (17). Lama4 and Lama5 genes are widely expressed by these 9 peripheral LNSC clusters (17). Changes to the Lama4/Lama5 ratios in the CR and around the HEVs are asso-

Conflict of interest: The authors have declared that no conflict of interest exists.

Submitted: November 18, 2019; **Accepted:** January 29, 2020; **Published:** April 13, 2020.
Reference information: *J Clin Invest*. 2020;130(5):2602–2619.
https://doi.org/10.1172/JCI135099.

ciated with immunity versus tolerance, with Lama4 associated with tolerance and Lama5 associated with immunity (8, 24). Alterations in laminin expression are associated with human diseases such as allergic asthma and inflammatory bowel disease (25, 26), suggesting laminins may be therapeutic targets.

We investigated the effect of LNSC Lama5 on T cell migration and function, and on immune responses during immunity and tolerance induction and after cardiac transplantation. Lama4 promoted, whereas Lama5 inhibited, migration of a variety of subsets of mouse and human T cells across endothelial cells. In a Lama5 conditional KO mouse model, *Lama5*$^{fl/fl}$ × *Pdgfrb*-Cre$^{+/-}$, depleting stromal Lama5 created a tolerogenic niche in the LN and hindered alloimmunity, through affecting LN structures, promoting T cell trafficking, and channeling T cell activation toward tolerance and away from inflammation. Blockade of Lama5 receptors using mAbs had similar effects and worked additively with Lama5 depletion to improve graft acceptance. Our study reveals the critical role of LNSC Lama5 in modulating LN structure and T cell behaviors, showing how the choice between immunity and tolerance is guided by stromal cell determinants of the LN microenvironment.

Results

Depleting LNSC Lama5 alters LN regulatory T cell distribution. We measured the expression of Lama4 and Lama5 in various cell types in mouse LNs by flow cytometry. Lama4 and Lama5 were widely expressed intracellularly and extracellularly in FRCs, BECs, and LECs (Supplemental Figure 1, A and B; supplemental material available online with this article; https://doi.org/10.1172/JCI135099DS1). Lama5 was also detected intracellularly in CD4$^+$ and CD8$^+$ T cells, B cells, and DCs (Supplemental Figure 1, C and D). These results are commensurate with reports showing that Lama5 can be secreted by stromal cells and lymphocytes (17, 22, 27).

To clarify the mechanisms of how laminin modulates immunity, and because complete genetic ablation of the *Lama5* gene caused embryonic lethality (28), we created a stromal cell *Lama5*-KO by breeding *Pdgfrb*-Cre$^{+/-}$ (29) with *Lama5*$^{fl/fl}$ mice (28). *Lama5*-floxed and *Pdgfrb*-Cre DNA sequences were confirmed by genotyping (Supplemental Figure 2), and *Pdgfrb*-Cre$^{-/-}$ × *Lama5*$^{fl/fl}$ (WT) mice were used as littermate controls. LNSCs were isolated and quantitative real-time PCR (qRT-PCR) showed that Lama5 transcripts were completely depleted in FRCs and partially depleted in BECs and LECs, but Lama4 was not affected (Figure 1A). There were no differences in Lama4 and Lama5 expression in CD4$^+$ and CD8$^+$ T cells, B cells, and DCs in WT and Lama5-KO mice (Supplemental Figure 3). By fluorescent immunohistochemistry, Lama5 was depleted in the CR and HEVs, but Lama4 was not affected, resulting a significant increase in the Lama4/Lama5 ratio. In contrast, neither Lama4 nor Lama5 was depleted in the spleen (Figure 1, B and C). There were no differences in the numbers or percentages of various leukocyte subsets, including CD3$^+$ and CD8$^+$ T cells, B cells, and DCs in the LNs, spleen, and thymus (Supplemental Figure 4), indicating no major shifts in cell numbers and distribution.

Because the Lama4/Lama5 protein ratio was associated with the choice of tolerance versus immunity and the induction of suppressive, regulatory, Foxp3$^+$ Tregs in the LNs (8), we assessed whether genetic ablation of stromal Lama5, which increased the ratio, would influence the number or distribution of Tregs. The natural Treg (nTreg, Foxp3$^+$Helios$^+$) percentage was slightly increased, but there was no significant difference in the percentage of total Tregs and peripherally induced Tregs (iTregs, Foxp3$^+$ Helios$^-$) in Lama5-KO compared with WT LN or spleen (Supplemental Figure 5). However, by immunohistochemistry, Tregs were significantly increased in the LN T cell zone (CD3$^+$), but not in the B cell zone (B220$^+$), germinal center (peanut agglutinin$^+$) (Figure 1D), or subcapsular sinus (Supplemental Figure 6). In the CR and around HEVs of Lama5-KO LNs, there were also more CD11c$^+$ DCs detected (Supplemental Figure 7, A and B), although no significant difference in the total LN percentage between WT and KO (Supplemental Figure 4). This observation is commensurate with our prior report that plasmacytoid DCs in the CR present alloantigen to induce iTregs (30).

Depleting Lama5 alters LN structures and molecules favorable for T cell migration. The number and size of HEVs (CD31$^+$PNAd$^+$) increased in Lama5-KO LNs, particularly in paracortex area (Figure 2, A and B). Transcripts for VEGF-A, VEGF-C, and VEGF-D, which are mediators of LN endothelial cell proliferation (31), were measured. VEGF-A mRNA was increased in Lama5-KO FRCs, while VEGF-C and VEGF-D were not affected (Figure 2C). Notably, the increased numbers of Tregs were highly colocalized with PNAd$^+$ HEVs in peripheral LNs (pLNs) and mesenteric LNs (mLNs) (Figure 2B and Supplemental Figure 8), suggesting that the increased Tregs may have accumulated due to enhanced migration through blood and/or retention within the CR. Hence, we analyzed the chemokines, including CCL19, CCL21, and CXCL12, which drive T cell entry into LNs through HEVs. In Lama5-KO mice, CXCL12 and CCL21 expression was increased around the CR of pLNs and mLNs (Figure 3A and Supplemental Figure 9), while CCL19 (Supplemental Figure 10), CXCL9, and CXCL10 (data not shown) showed no differences. CCL21 and CXCL12 mRNA increased in FRCs but not in BECs and LECs (Figure 3A). FRCs express intercellular adhesion molecule-1 (ICAM-1), vascular cell adhesion molecule-1 (VCAM-1), and mucosal vascular addressin cell adhesion molecule-1 (MAdCAM-1), which play important roles in T cell migration (32). In the LNs of Lama5-KO mice, VCAM-1 protein expression was increased in the CR and around HEVs, and the mRNAs encoding VCAM-1 and ICAM-1, but not MadCAM-1, were increased in FRCs (Figure 3, B and C). Taken together, these results showed that depletion of Lama5 in LNSCs created a favorable microenvironment for Treg enrichment, including more HEVs, enhanced chemokine expression, and increased VCAM-1, allowing for increased Treg presence in the cortical T cell zones.

Lama5 regulates T cell transendothelial migration through the receptors α6 integrin and α-dystroglycan. In order to delineate the direct effects of laminins on migration of various mouse and human T cells, different in vitro cell migration models and conditions were included. We firstly investigated the effects of the 2 main laminin isoforms, α4β1γ1 (laminin 411) and laminin α5β1γ1 (laminin 511), on CD4$^+$ T cell migration on laminin-coated plates by measuring length (distance migrated) and velocity with real-time live imaging. Laminin 411 promoted both increased length of migration pathways and velocity, while laminin 511 inhibited these responses (Figure 4A and Supplemental Videos 1–4). We next studied the role of the receptors α6 integrin and α-dystroglycan (αDG) in Lama5-regulated T cell migration. The receptor α6

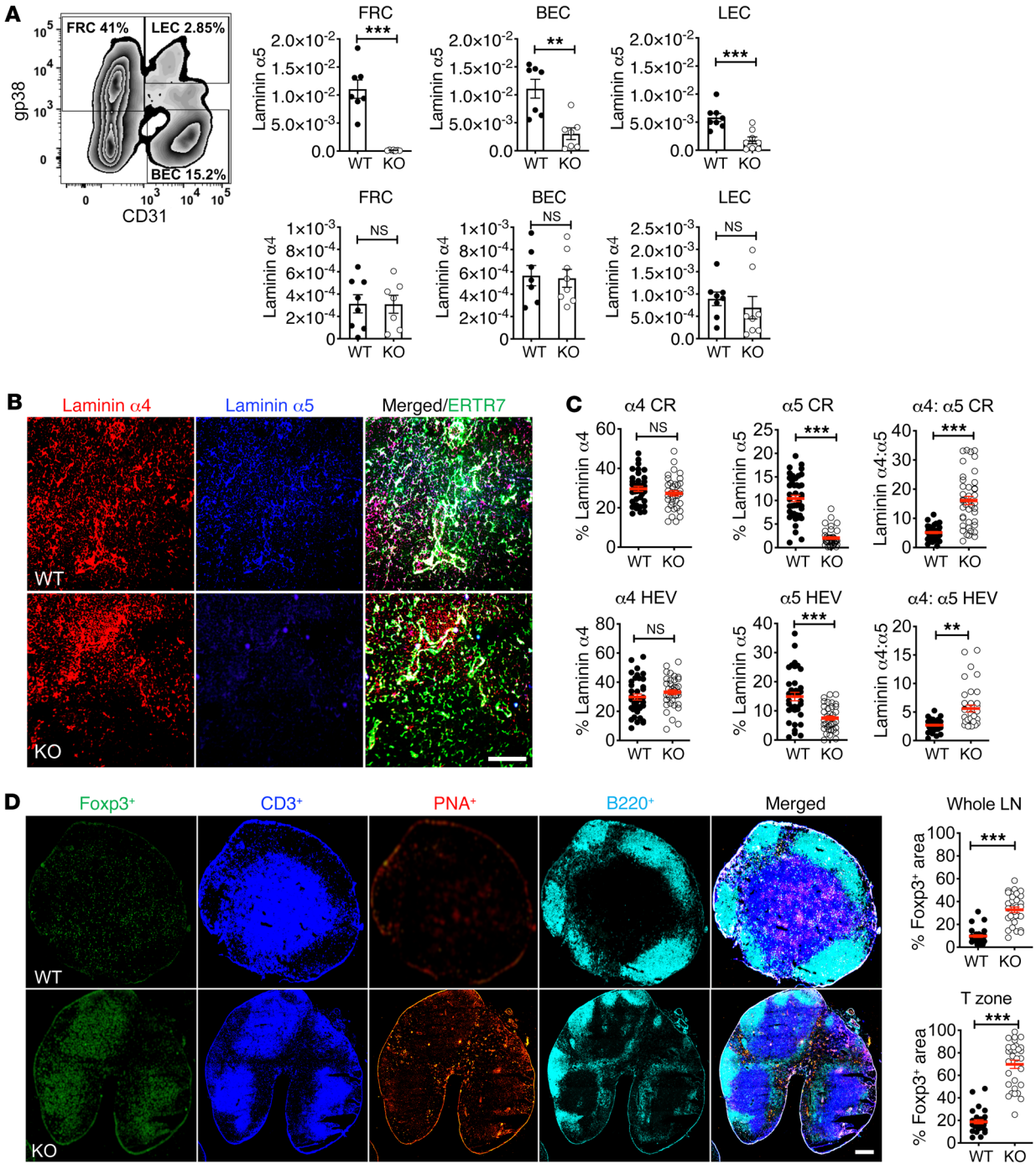

Figure 1. Characterization of Lama5 conditional KO mice. (**A**) Lama4 and Lama5 gene expression in FRCs, BECs, and LECs in Lama5-KO and WT mice. Stromal cell subsets sorted from LNs of Lama5-KO and WT mice; Lama4 and Lama5 transcripts relative to cyclophilin A measured by qRT-PCR (n = 7). (**B** and **C**) Lama4 and Lama5 expression in peripheral LNs from Lama5-KO and WT mice. (**B**) LN sections stained for Lama4 and Lama5; representative images at ×20 original magnification. Scale bar: 100 μm. (**C**) Percentages of Lama4- and Lama5-positive areas, and Lama4/Lama5 ratios in the CR and around HEVs (n = 30). (**D**) pLNs stained for Foxp3, CD3, peanut agglutinin, and B220. Left: Representative images. Scale bar: 200 μm. Right: Quantification of Tregs in whole section and T cell zones (n = 30). In all panels, at least 3 independent experiments, 3 mice/group, 3 LNs/mouse, 3 sections/LN and 3–5 fields/section. Data are presented as mean ± SEM. $^{**}P < 0.01$, $^{***}P < 0.001$ by unpaired, 2-tailed Student's t test.

integrin has been widely recognized for being expressed on lymphocytes and bone marrow cells (27, 33). αDG gene expression was confirmed in various T cell subsets (Figure 4B). Pretreating CD4$^+$ T cells with blocking mAbs against α6 integrin or αDG prevented laminin 511 inhibitory effects and preserved length and velocity (Figure 4C), indicating that laminin 511 affects CD4$^+$ T cell migration independently through both receptors, α6 integrin and αDG.

CD4$^+$ T cells were cultured on laminin 411–coated and/or 511–coated plates and cell attachment was measured. Both anti-CD3–activated and nonactivated cells bound more to laminin 511

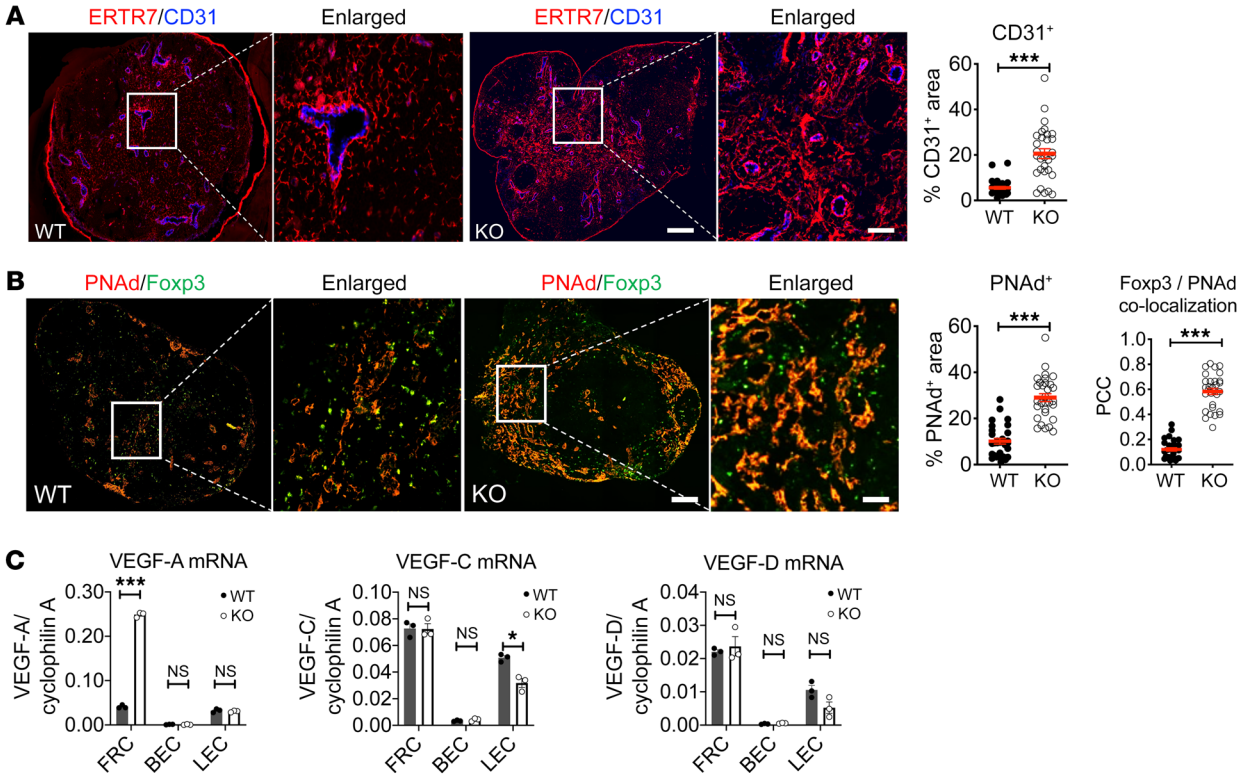

Figure 2. Depleting stromal Lama5 increases LN Tregs and HEVs. (**A**) LN stained for ER-TR7 and CD31. (**B**) LN stained for PNAd and Foxp3 and colocalization of Foxp3 and PNAd analyzed by Pearson's correlation coefficient (PCC). Scale bars: 200 μm (left) and 50 μm (right). In whole-section images, original magnification is ×20. Left panels, representative images; right panels, staining percentages (n = 30). (**C**) VEGF-A, VEGF-C, and VEGF-D gene expression in FRCs, BECs, and LECs in Lama5-KO and WT mice (n = 3). Data (mean ± SEM) are representative of 3 independent experiments with 3 mice/group, 3 LNs/mouse, 3 sections/LN, and 3–5 fields/section. *P < 0.05; ***P < 0.001 by unpaired, 2-tailed Student's t test.

than 411; however, the binding was only transient, not influenced by anti-CD3 activation, and returned to baseline within 60 minutes (Figure 4D). With the addition of CCL21 to stimulate chemokine receptors, cell attachment was increased, but the effects of laminins were diminished (Figure 4D). Similarly, there was no increased binding under shear flow conditions in the presence of BECs (Figure 5, H–J). Blocking α6 integrin or αDG did not inhibit the transient T cell binding (data not shown). Together, these data showed that inhibition of migration by laminin 511 was not due to simple high affinity binding to Lama5.

Transwell assays were conducted using a Boyden chamber coated with BEC monolayers and a CCL21 gradient (Figure 5A). Naive CD4$^+$, T memory, T effector, nTreg, iTreg, and CD8$^+$ T cell subsets behaved similarly: laminin 411 promoted and laminin 511 inhibited their migration (Figure 5, B and C). The combination of 411 plus 511 resulted in mutual inhibitory effects. The Lama5 inhibitory effects were attenuated with blocking α6 integrin or αDG mAbs (Figure 5B and Supplemental Figure 11), indicating that many different T cells recognize Lama5 through α6 integrin and αDG. Additionally, laminin 421 and 521 trimers displayed similar stimulatory and inhibitory effects as laminin 411 and 511, respectively (Figure 5D), indicating that the laminin α chain was responsible for these functions. Moreover, laminin 411 promoted, whereas 511 suppressed, the transendothelial migration (TEM) of human Tregs and activated CD4$^+$ T cells, which also recognized laminin 511 through α6 integrin and αDG (Figure 5, E and F).

In vitro shear flow was performed using the Bioflux system to model in vivo blood vessel laminar flow (Figure 5G). The flow channel was coated with a BEC monolayer along with CCL21 over a coating of laminin 411 and/or 511. Shear was applied to the channels by laminar flow and T cells attaching to the endothelial layer were recorded in intervals by real-time imaging. As compared with the PBS-coated control group, laminin 411 favored the attachment and TEM of CD4$^+$ T cells and iTregs, while laminin 511 inhibited this response (Figure 5H). The laminin 511 inhibition was attenuated by adding laminin 411 to the coating or by pretreating the T cells with mAbs against α6 integrin or αDG (Figure 5I). A turbulent-flow device supplying higher shear force (4 dynes/cm^2) (34) was used to confirm the effects of laminins 411 and 511 on TEM. Laminin 411 promoted, but laminin 511 inhibited, both CD4$^+$ and CD8$^+$ T cell TEM (Figure 5J). Overall, these data showed that Lama4 promoted, whereas Lama5 inhibited, many parameters of T cell TEM toward chemokine signaling, and T cells recognize laminin 511 through α6 integrin and αDG.

Lama5 restricts CD4$^+$ T cell and Treg migration in vivo. Because the LNs of Lama5-deficient mice contained more chemokines, cell adhesion molecules, HEVs, and Tregs in the CR, and because laminins regulated numerous aspects of T cell migration, we hypothesized that laminins directly regulated migration of T cells and Tregs to the HEVs and CR. To test this, naive CD4$^+$ T cells and iTregs were labeled with eFluor 670 and CFSE, respectively, and adoptively transferred into Lama5-KO and WT mice. After 16 hours, T cell entry into LNs

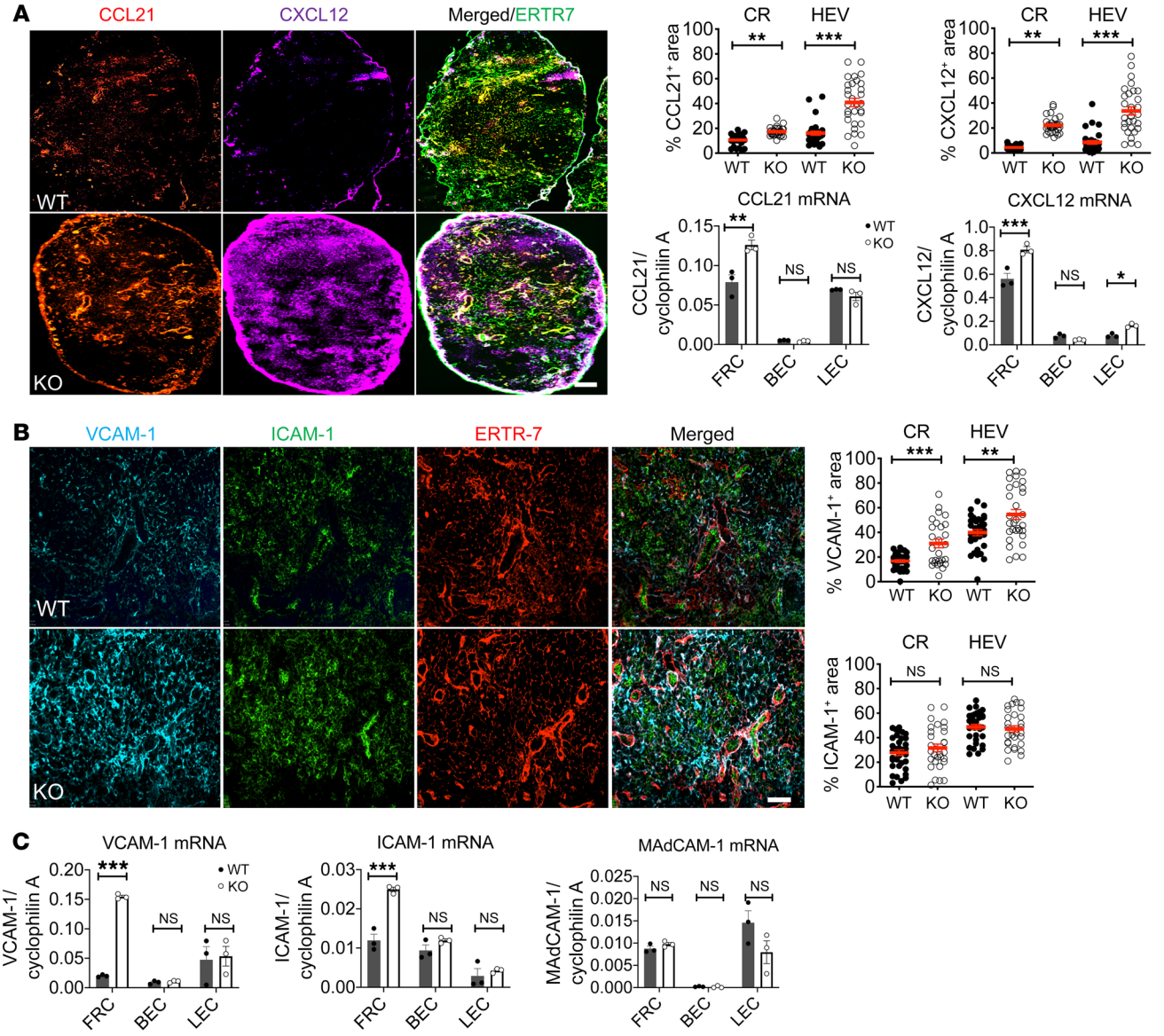

Figure 3. Depleting stromal Lama5 increases CCL21, CXCL12, and VCAM-1. (**A**) Left and upper right: CCL21 and CXCL12 protein expression in the CR and around HEVs (n = 30). Scale bar: 200 μm; in whole-section images, original magnification is ×20. Lower right: CCL21 and CXCL12 gene expression in FRCs, BECs, and LECs in Lama5-KO and WT mice (n = 3). (**B**) VCAM-1 and ICAM-1 protein expression in the CR and around HEVs (n = 30). Scale bar: 50 μm. (**C**) VCAM-1, ICAM-1, and MAdCAM-1 gene expression in FRCs, BECs, and LECs in Lama5-KO and WT mice (n = 3). Data (mean ± SEM) are representative of 3 independent experiments with 3 mice/group, 3 LNs/mouse, 3 sections/LN, and 3–5 fields/section. *P < 0.05; **P < 0.01; ***P < 0.001 by unpaired, 2-tailed Student's t test.

was evaluated through immunohistochemistry. In Lama5-KO mice, transferred naive CD4$^+$ T cells and iTregs were both increased 2-fold in the CR and 4-fold in HEVs compared with WT (Figure 6A). To test T cell retention in LNs, blocking mAbs against CD62L were administered 18 hours after T cell transfer. The cells remaining in LNs were assessed 18 hours after mAb administration. The results showed that there was CD4$^+$ T cell egress, with cells egressing slightly more from Lama5-KO compared with WT LNs. In contrast, iTregs were relatively retained in LNs and there was no difference between WT and KO LNs (Supplemental Figure 12). Overall, these results suggest that the relatively high concentration of CD4$^+$ T cells or Tregs in the CR and HEVs of Lama5-KO LNs was due primarily to increased migration into the LNs rather than increased retention.

Naive CD4$^+$ T cells and iTregs were pretreated with blocking mAbs against αDG or α6 integrin before adoptive transfer to WT recipients. Both blocking mAbs significantly increased naive CD4$^+$ T cell and iTreg migration into LNs compared with the isotype controls (Figure 6B). More transferred naive CD4$^+$ T cells and iTregs were detected in the CR and around HEVs (Figure 6C). These findings further demonstrated that Lama5 regulates T cell entry into LNs via receptors αDG and α6 integrin. Our results also show that these mAbs do not deplete T cells, so that their immunomodulatory effects (*vide infra*) were not due to simple depletion of T cells. Indeed, i.v. injection of anti-αDG or anti–α6 integrin resulted in increased numbers of Tregs and CD4$^+$ T cells in the CR and around HEVs (Figure 7, A–D), while there were no significant differences

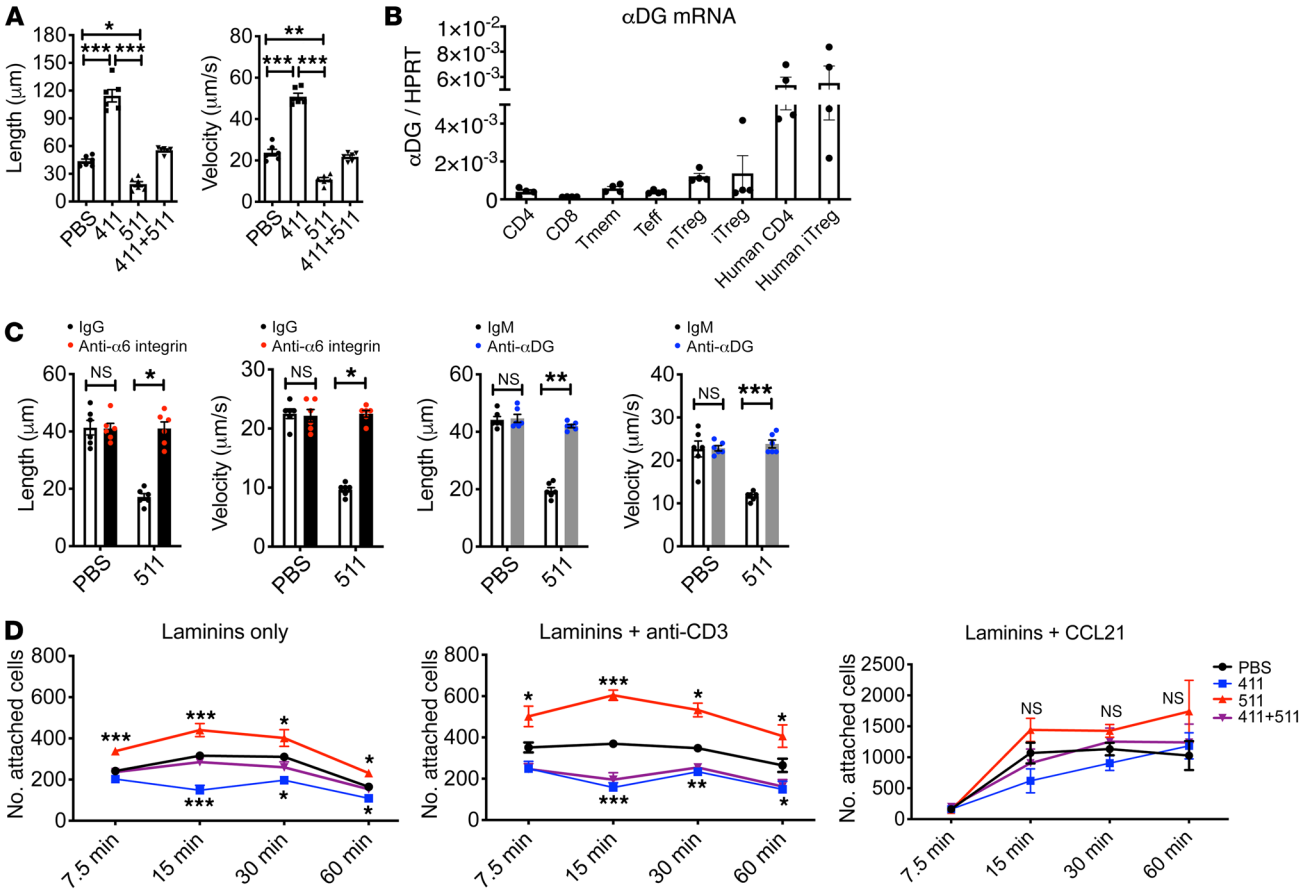

Figure 4. Lama5 regulates T cell migration via α6 integrin and αDG. (**A**) CD4⁺ T cell track length and velocity migrating on surfaces coated with laminin α4β1γ1 (laminin 411) and/or α5β1γ1 (laminin 511) (2 μg/mL each) measured with real-time live imaging (n = 6). (**B**) αDG gene transcripts in various T cell subsets relative to hypoxanthine phosphoribosyltransferase (HPRT) measured by qRT-PCR (n = 4). (**C**) Track length and velocity of CD4⁺ T cells treated with blocking mAbs against α6 integrin (10 μg/mL, isotype IgG) or αDG (5 μg/mL, isotype IgM) (n = 6). (**D**) CD4⁺ T cell binding to 96-well flat-bottom plates coated with laminin 411 and/or 511 (2 μg/mL each), plus anti-CD3 (50 μg/mL) or CCL21 (500 ng/mL) (n = 8). Data (mean ± SEM) are representative of 3 experiments. $^*P < 0.05$; $^{**}P < 0.01$; $^{***}P < 0.001$ by 1-way ANOVA with Tukey's multiple-comparisons test.

in CD8⁺ T cells, DCs, or B cells (Supplemental Figure 13). These results indicated that systemically blocking Lama5 receptor αDG or α6 integrin altered the trafficking of endogenous CD4⁺ T cells and nTregs without depletion of, or interference with, other leukocytes.

Overall, the in vivo migration of CD4⁺ T cells and iTregs from blood to LNs was facilitated through either genetically depleting the LNSC Lama5 gene or pharmacologically blocking Lama5 receptors. In this niche, T cells migrated through and interacted with Lama5 via αDG and anti–α6 integrin, and Lama5 was a key component of the microenvironment that restricted T cell migration.

Lama5 regulates antigen-specific T cell responses to alloantigen. The effect of Lama5 on antigen-specific CD4⁺ T cell responses during immunity and tolerance induction was assessed. Lama5-KO and WT (all C57BL/6 [H-2^b] background) mice were immunized with BALB/c (H-2^d) donor-specific splenocyte transfusion (DST) or tolerized with anti-CD40L mAb plus DST. Recipients had adoptive transfer from CD45.1 T cell receptor–transgenic (TCR-Tg) CD4⁺ T cells from TEa mice that recognize donor I-E^d (Ea antigen) presented by recipient I-A^b (35). After 3 and 5 days, TEa T cell enrichment, activation, and polarization in pLNs, mLNs, and spleen were analyzed. Under both immune and tolerant conditions, more transferred cells were detected in secondary lymphoid organs (SLOs) than in naive conditions without DST or anti-CD40L after 3 days of injection. Notably, there were also more TEa cells in Lama5-KO than in WT SLOs (Figure 8A). In immune and tolerant conditions more transferred cells were observed in the KO LNs around HEVs (Figure 8B). In immunity, the activation of alloantigen-specific CD4⁺ T cells determined by CD44^{hi}CD69⁺ expression was lower in Lama5-KO LNs compared with WT, 3 and 5 days after injection. There was a similar trend in tolerogenic conditions (Figure 9A), indicating that depleting Lama5 may have an inhibitory effect on T cell activation. In tolerance and immunity, there was a higher Treg/Th17 ratio in Lama5-KO SLOs, with significant values in tolerance. This indicates that depleting stromal Lama5 favored Treg differentiation (Figure 9B). These results showed that stromal Lama5 functioned in vivo during the response to alloantigen, and deficiency of Lama5 created a tolerogenic niche with more Tregs.

Depletion of LNSC Lama5 promotes tolerance. Lama5-KO and WT mice received cardiac allografts from BALB/c donor mice. Without immunosuppression, all allografts were acutely rejected by both groups with identical kinetics (median survival time

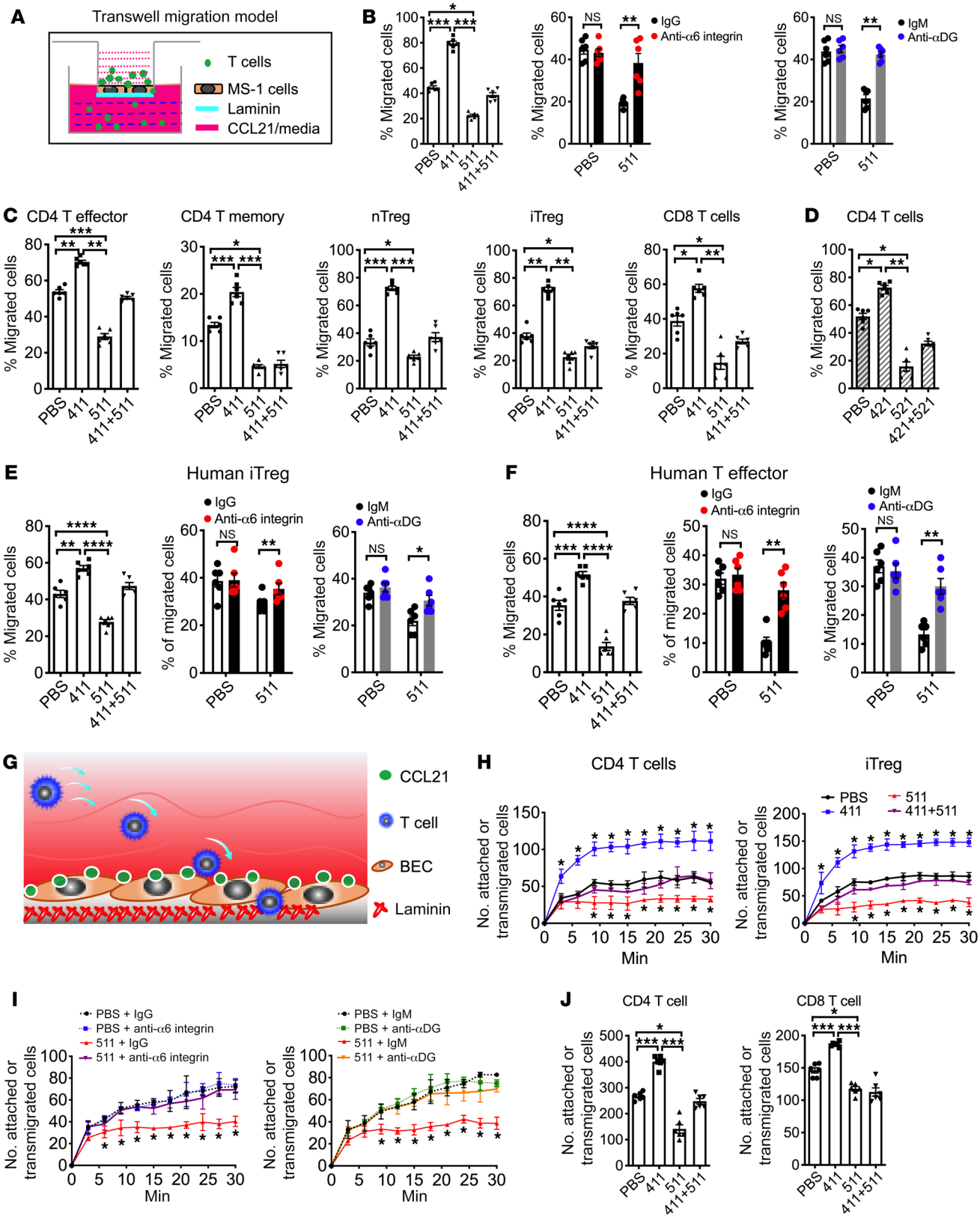
A
Transwell migration model
T cells
MS-1 cells
Laminin
CCL21/media
B
% Migrated cells
PBS
411
511
411+511
IgG
Anti-α6 integrin
IgM
Anti-αDG
NS
C
CD4 T effector
CD4 T memory
nTreg
iTreg
CD8 T cells
D
CD4 T cells
421
521
421+521
E
Human iTreg
% of migrated cells
F
Human T effector
G
CCL21
T cell
BEC
Laminin
H
CD4 T cells
iTreg
No. attached or transmigrated cells
Min
I
PBS + IgG
PBS + anti-α6 integrin
511 + IgG
511 + anti-α6 integrin
PBS + IgM
PBS + anti-αDG
511 + IgM
511 + anti-αDG
J
CD4 T cell
CD8 T cell

Figure 5. Lama5 inhibits CD4⁺ T cell and iTreg transendothelial migration via α6-integrin and αDG. (**A**) Schematic representation of transwell assay. Boyden chambers were coated with 30 μg laminin; BECs line MS-1 monolayers coated on inserts. T cells (2×10^5) were loaded into the upper chamber, and 500 ng/mL CCL21 was added to the bottom chamber. Percentage of cells that migrated to the bottom chamber was determined after 3 hours. (**B**) Percentage of migrated CD4⁺ T cells; anti–α6 integrin or anti-αDG pretreatment of T cells. (**C**) Migration of CD4⁺ T effector and memory cells, natural and induced Tregs, and CD8⁺ T cells. (**D**) CD4⁺ T cell migration across laminin 421 or/and laminin 521. (**E** and **F**) Migration efficiency of human CD4⁺ iTregs and T effector cells; anti–α6 integrin or anti-αDG pretreatment. $n = 6$ (**B**–**F**). (**G**) Schematic representation of T cell migration in laminar flow channels with shear force using BioFlux. Laminar flow channels were coated with 30 μg/mL laminin 411 and/or 511. BEC MS-1 cells were grown to confluence and 500 ng/mL CCL21 was passed through the laminar flow channels and incubated at 37°C for 6 hours. CD4⁺ T cells or iTregs were passed through the flow channels at 0.5 dynes/cm². (**H**) Adherence of CD4⁺ T cells or iTregs imaged at 1-minute intervals for 30 minutes. (**I**) CD4⁺ T cells pretreated with anti–α6 integrin or anti-αDG. $n = 3$ (**H** and **I**). (**J**) Adherence of CD4⁺ T cells or CD8⁺ T cells after 3 minutes of cell perfusion over BEC layers in a flow device ($n = 6$). Data are presented as mean ± SEM from 3 independent experiments. *$P < 0.05$; **$P < 0.01$; ***$P < 0.001$; ****$P < 0.0001$ by 1-way ANOVA with Tukey's multiple-comparisons test.

[MST] = 6.5 days), indicating that the conditional KO does not affect acute allograft rejection significantly (Figure 10A). Next, we assessed clinically relevant, but nontolerogenic, immunosuppressive protocols. Starting on the day of transplantation, mice received either tacrolimus (2 mg/kg/d s.c.) or a single dose of anti-CD40L mAb (250 μg i.v.). Graft function was monitored until rejection. Lama5-KO recipients treated with tacrolimus had significantly longer survival than WT (MST 89 vs. 27.5 days, $P < 0.002$; Figure 10B). A trend for prolongation of graft survival was also observed with anti-CD40L (MST 155 vs. 91 days, $P = 0.07$; Figure 10C). Therefore, conditional deletion of LN Lama5 promoted longer graft acceptance with single-immunosuppression regimens with a calcineurin inhibitor or costimulatory blockade treatment.

Because Lama5 regulates T cells through αDG or α6 integrin, and because not all Lama5 was depleted in the conditional KO, we hypothesized that blocking these receptors would be immunosuppressive and have additive effects in Lama5-KO mice. As noted above, these antibodies were not depleting, so that any influence on graft survival would not be due to depletion of effector cells. Lama5-KO and WT recipients received anti–α6 integrin (10 μg i.v., isotype IgG) or anti-αDG (10 μg i.v., isotype IgM) mAb every 3 days. Compared with the isotype control group, WT recipients treated with anti–α6 integrin had a small but significant prolongation of allograft survival (MST 10 vs. 7 days, $P < 0.001$), while Lama5-deficient recipients displayed further prolongation (MST 12 days, $P < 0.05$, compared with WT; Figure 10D). Lama5-KO mice treated with αDG had the most prolonged allograft survival (MST 13 vs. 7 days, $P < 0.003$; Figure 10E), as compared with WT recipients, which showed similar allograft survival to the isotype controls (MST 7 days). Administration of anti–α6 integrin plus anti-αDG to WT recipients increased MST up to 15 days compared with isotype controls (MST 8 days). Notably, the Lama5-KO recipients treated with anti-αDG plus anti–α6 integrin displayed a further increase in MST to 27.5 days (Figure 10F). These observations indicated that depletion of LNSC Lama5 and systemic blockade of the laminin 511 receptors αDG and/or α6 integrin prolonged allograft survival and those strategies work additively.

We also investigated the influence of blocking Lama5 receptors together with tacrolimus. Mice receiving tacrolimus plus anti–α6 integrin had longer graft survival than controls (MST 67.5 vs. 28.5 days, $P < 0.005$; Figure 10G). Similarly, tacrolimus plus αDG treatment also significantly increased graft survival (MST from 19 to 63.5 days, $P < 0.001$; Figure 10H). These results are commensurate with genetically depleting stromal Lama5 (Figure 10B), again confirming the role of Lama5 in chronic graft alloimmunity.

Because stromal Lama4 and Lama5 are expressed around blood vessels (36), we asked if there were changes in their distribution in the allograft as a result of the different treatments. As compared with healthy BALB/c hearts, Lama4 was slightly increased (2-fold), but Lama5 increased more dramatically by 4-fold in the rejected heart, leading to a reduced Lama4/Lama5 ratio (Figure 11, A and B). Further, the grafts of recipients without immunosuppressor were rejected at day 9 of transplantation. In rejected grafts, Lama5 increased 8-fold compared with normal hearts and 2-fold versus nonrejected grafts (day 6), while Lama4 did not show further increase compared with nonrejected grafts, leading to a decreased Lama4/Lama5 ratio. Nevertheless, in the anti-CD40L–treated recipients, grafts were not rejected at day 9 and the Lama4 and Lama5 levels were comparable to that of day6 recipients. Overall, these results showed that a decreased Lama4/Lama5 ratio in tissues was also associated with the severity of rejection.

LNSC Lama5 regulates alloantigen-specific T cell responses during transplantation. On the day of cardiac transplantation, CD45.1⁺CD4⁺ TEa cells were transferred into the recipients treated with anti-CD40L. After 3 or 5 days, TEa cell migration, activation, and differentiation within recipient SLOs were analyzed. At day 3 after transplantation, more TEa cells were detected in SLOs compared with nontransplanted controls injected with TEa cells only, and more TEa cells were detected in Lama5-KO than in WT recipient SLOs (Figure 12A). TEa cell activation marked by CD44^{hi}CD69⁺ was decreased in Lama5-KO recipient LNs (Figure 12B). Higher Treg/Th17 ratios were detected in Lama5-KO recipient LNs (Figure 12C). Together, those results demonstrated that LNSC Lama5 regulated antigen-specific CD4⁺ T cell migration and activation, and played a role in balancing tolerance versus immunity, thereby affecting allograft survival and transplantation outcomes.

Discussion

We established a conditional Lama5-KO mouse model in which Lama5 transcripts were depleted completely in FRCs, and partially in BECs and LECs. The Lama5 protein was decreased and the Lama4/Lama5 protein ratios were increased in the CR and around HEVs, with upregulated numbers of Tregs, expression of the cell migration–related chemokines CCL21 and CXCL21, and expression of VCAM-1 also in the CR and around the HEVs (Figure 13). Under both static and shear stress flow conditions, the TEM of various mouse and human T cell subsets was enhanced by laminin 411. In contrast, laminin 511 inhibited T cell TEM. In vivo LN trafficking was regulated by Lama5 through the T cell receptors α6 integrin and αDG, and inhibiting these receptors also resulted in enhanced migration of Tregs into the CR, similarly to genetic ablation of Lama5. Depleting stromal Lama5 promoted antigen-specific T cell migration into the LNs, interfered with their activation, and altered their differentiation under both immune and tolerant conditions,

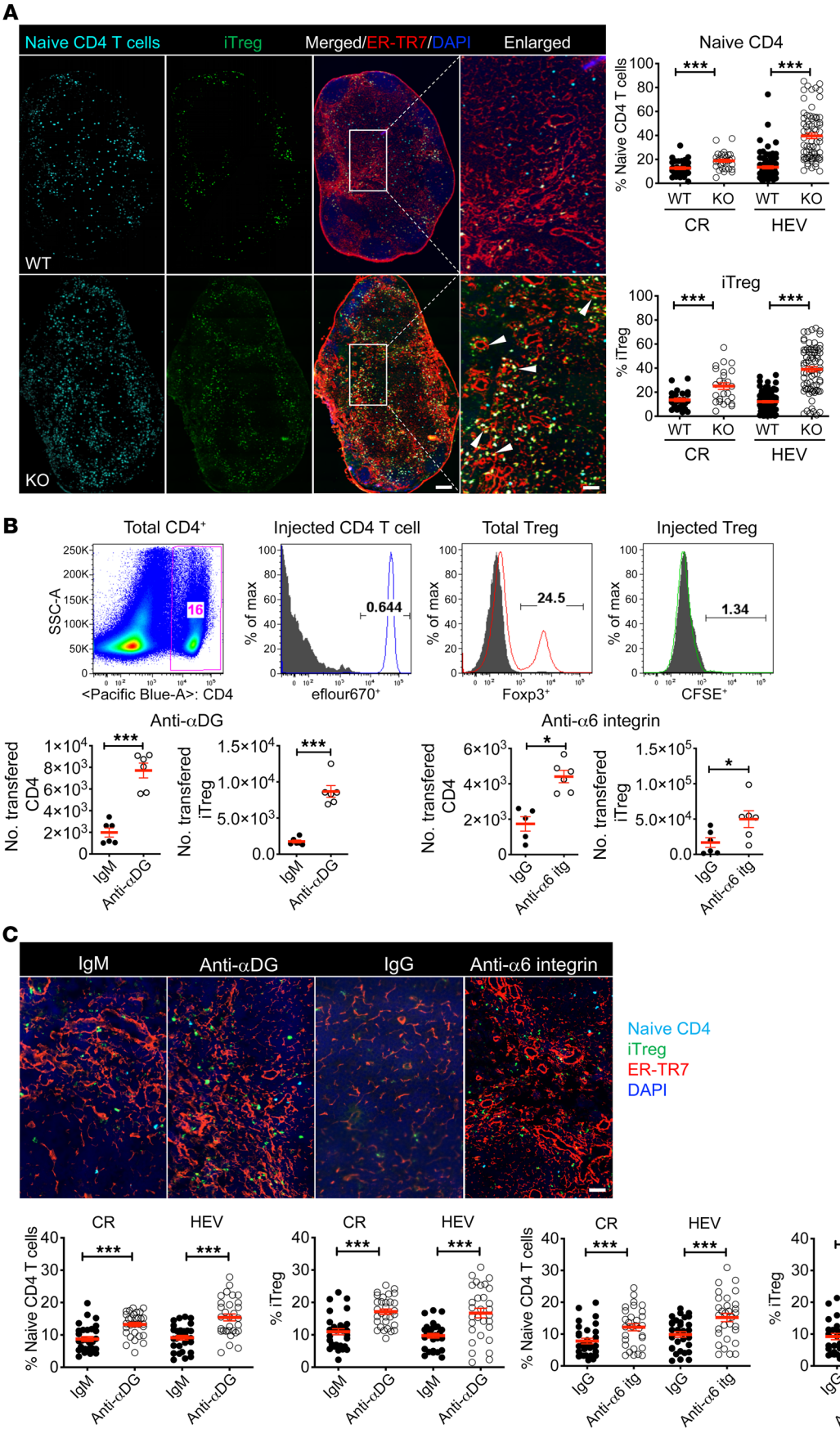

Figure 6. Lama5 regulates CD4⁺ T cell and Treg entry into LNs via αDG and α6 integrin. (**A**) CFSE-labeled iTregs (2×10^5) and 2×10^6 eFluor 670–labeled CD4⁺ cells transferred i.v. to Lama5-KO or WT mice. After 16 hours, LNs were stained for ER-TR7 and with DAPI and analyzed for the transferred cells. Left panels: Representative whole-section images (original magnification, ×20); arrowheads indicate HEVs. Scale bars: 200 μm (left) and 50 μm (right). Right panels: Quantification of naive CD4⁺ T cells and iTregs in the CR and HEVs ($n = 30$). (**B** and **C**) T cells pretreated with anti-αDG (2.5 μg mAb/10^6 cells, isotype IgM) or anti–α6 integrin (itg) (5 μg mAb/10^6 cells, isotype IgG) before transfer. After 16 hours, LNs were harvested for immunohistochemistry and flow cytometry. (**B**) Upper panels: Gating strategy. Lower panels: Number of transferred naive CD4⁺ T cells (eFluor 670⁺) and iTregs (CFSE⁺) per 1×10^6 total CD4⁺ T cells or total Foxp3⁺ cells ($n = 6$). (**C**) Upper panels: Representative scanning images (original magnification, ×20). LNs were stained for ER-TR7 and with DAPI and analyzed for transferred cells. Scale bar: 50 μm. Lower panels: Quantification of transferred naive CD4⁺ T cells (eFluor 670⁺) and iTregs (CFSE⁺) in the CR and HEVs ($n = 30$). Data (mean ± SEM) are from 3 independent experiments with 3 mice/group. For immunohistochemistry, 5 LNs/mouse, 3 sections/LN, and 3–5 fields/section. $^*P < 0.05$; $^{***}P < 0.001$ by unpaired, 2-tailed Student's t test.

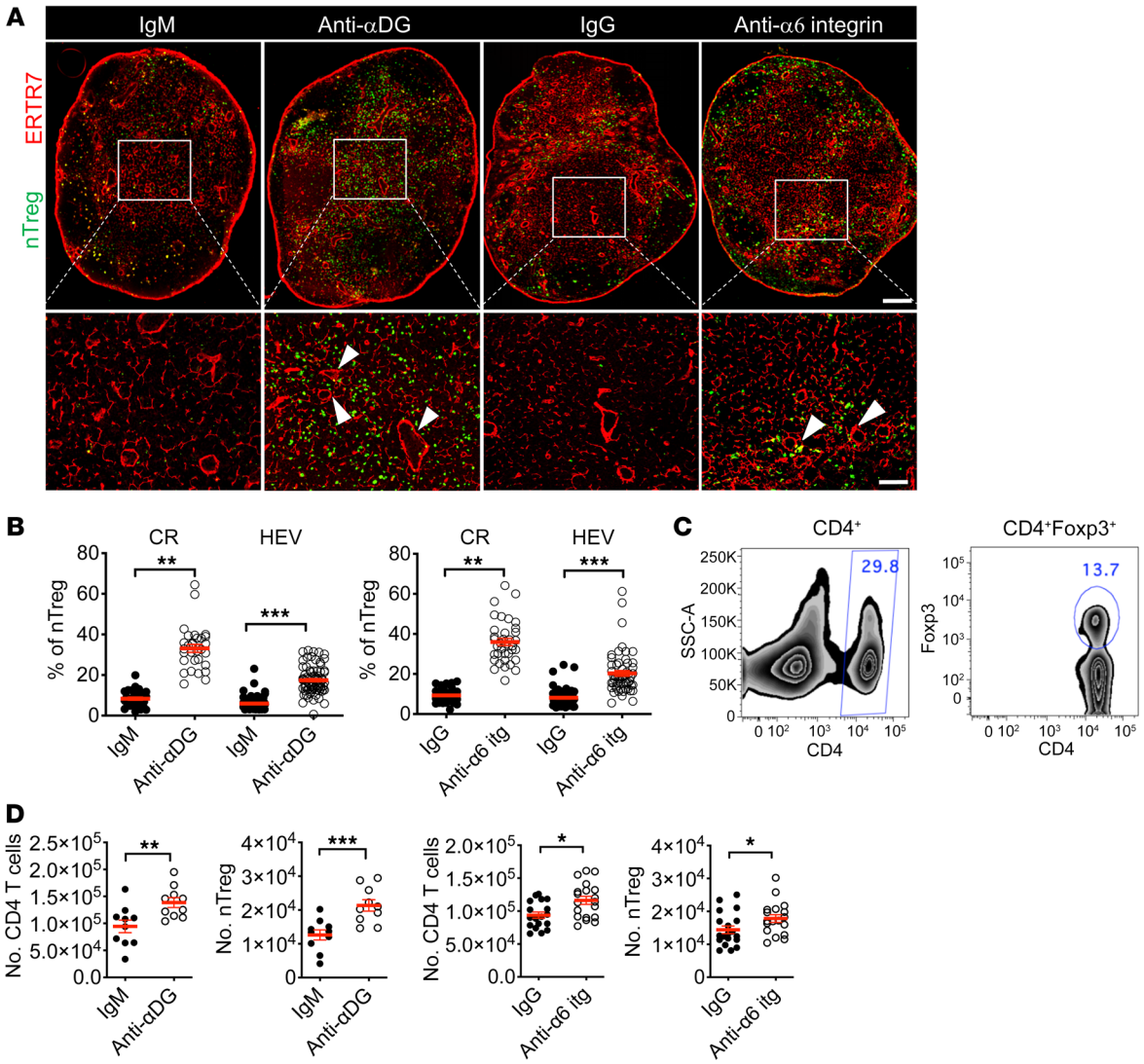

Figure 7. Systemically blocking αDG and α6 integrin increases CD4⁺ T cell and nTreg accumulation in LNs. C57BL/6 mice were injected i.v. with 10 μg anti-αDG (isotype IgM) or 10 μg anti–α6 integrin (itg) (isotype IgG); LNs were harvested after 16 hours. (**A**) Representative whole-section images (original magnification, ×20). Scale bars: 200 μm (upper) and 50 μm (lower). Sections were stained for Foxp3 and ER-TR7; arrowheads indicate HEVs. (**B**) Quantification of nTregs in the CR and HEVs (n = 30). (**C**) Gating strategy for CD4⁺ T cells and nTregs; values show population percentage. (**D**) Number of CD4⁺ T cells and nTregs in each LN (n = 10). Data (mean ± SEM) are based on at least 3 independent experiments with 3 mice/group. For immunohistochemistry, 3 LNs/mouse, 3 sections/LN, and 3–5 fields/section. For flow cytometry, 5 LNs/mouse. *P < 0.05, **P < 0.01, ***P < 0.001 by unpaired, 2-tailed Student's t test.

and during allograft transplantation. Prolonged allograft acceptance was obtained by modulating Lama5 expression genetically or function pharmacologically, with both strategies working additively. Together, our study illustrated that LNSC Lama5 regulated the immune response through T cell migration and function.

Depleting LNSC Lama5 did not change total CD4⁺ T cell, CD8⁺ T cell, B cell, or DC percentages in the thymus, LNs, or spleen. However, depleting stromal Lama5 led to increased type 2 innate lymphoid cells (ILC2s) but decreased ILC3s in peripheral LNs (Supplemental Figure 14). LNSC percentages were also not altered, but HEV structures marked by CD31 and PNAd were increased in the Lama5-KO LNs. HEV neogenesis requires the interaction between lymphoid tissue organizer (LTo) cells and lymphoid tissue inducer (LTi) cells. During the interaction, the endothelial LTo cells express adhesion molecules like ICAM-1 and VCAM-1 and chemokines including CCL19 and CCL21 to attract the LTi cells (37, 38). We showed that CCL21 and VCAM-1 were upregulated in Lama5-KO LNs, which may be involved in the LTo-LTi cell interaction and promote the enhanced generation of HEVs (39). Further, HEV maintenance relies on CD11c⁺ DCs (40–43) producing VEGF to induce HEV growth (43) and also stimulating FRCs to secrete VEGF in an LTβR-dependent manner (31). DC migration from the blood through HEVs relies on HEVs expressing CCL21 (30), while Lama5 suppresses DC motility (36). The present study showed that depleting stromal Lama5 upregulated CCL21 and more CD11c⁺ DCs were found around HEVs (Supplemental Figure 7, A and B). The increased CCL21 may facilitate DC recruitment to the LN paracortex and thus promote HEV neogenesis. Increased complexity of ER-TR7⁺ fibers branching around the HEV is associated with more Tregs in the CR, enhanced tolerance,

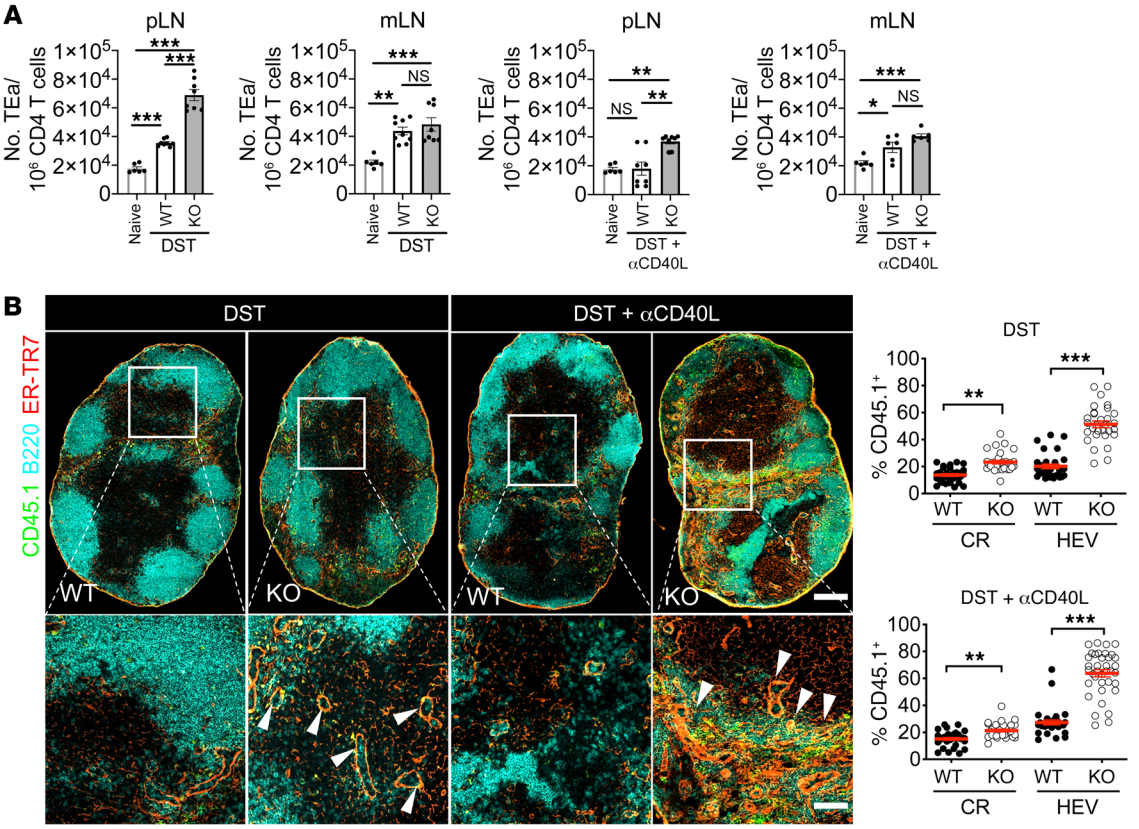

Figure 8. LN stromal Lama5 regulates antigen-specific CD4⁺ T cell distribution in LNs in immunity and tolerance. CD45.1⁺CD4⁺ TEa cells (1×10^6) were injected i.v. into immune (plus 1×10^7 DST) or tolerant (plus 1×10^7 DST and 250 μg anti-CD40L) Lama5-KO and WT mice. WT mice only injected with TEa cells served as negative control (naive). (**A**) Number of TEa cells out of 1×10^6 CD4⁺ T cells in LNs 3 days after injection (n = 6–8). (**B**) Left panels: Representative whole-section images (original magnification, ×20). Scale bars: 200 μm (upper) and 50 μm (lower). LNs were harvested 3 days after injection and sections stained for ER-TR7, B220, and CD45.1; arrowheads indicates HEVs. Right panels: Quantification of TEa cells (CD45.1⁺) in the CR and HEVs (n = 30). Data (mean ± SEM) are representative of 2 independent experiments. For immunohistochemistry, 5 LNs/mouse, 3 sections/LN, and 3–5 fields/section. For flow cytometry, 5 LNs/mouse. *$P < 0.05$; **$P < 0.01$; ***$P < 0.001$ by 1-way ANOVA with Tukey's multiple-comparisons test for multiple-variable differences (**A**) or unpaired, 2-tailed Student's t test for single-variable differences (**B**).

and prolonged allograft survival (44), suggesting the increased HEV structures and enhanced lymphocyte trafficking work positively to promote immune regulation and tolerance. Taken together, our results demonstrated that depleting Lama5 in stromal cells, particularly in FRCs, affected specific LN structures that resulted in increased T cell and Treg migration to the LNs.

The CCR7-CCL19/CCL21 axis is the primary signaling driving LN homing, including naive T cells, Tregs, and DCs (45, 46). Both CCL21 and CXCL12 play crucial roles in TEM and intranodal distribution of T cells (47). CCL21 is abundantly produced by HEVs, while CXCL12 is mainly produced by FRCs (48). This is supportive of our data showing that CCL21 is primarily located around HEVs and CXCL12 is predominantly distributed in the CR. After L-selectin–regulated rolling and tethering, CCL21 immobilized on the HEV luminal surface by heparan sulfates is responsible for the activation-induced arrest of lymphocytes, as well as the subsequent TEM (49). CCL21 triggers LFA1 activation on the rolling lymphocytes, thereby transitioning to adhesion status of the lymphocytes (48). Here we detected greater numbers of Tregs in Lama5-KO CR and around HEVs. In Lama5-KO LNs, the chemokines CCL21 and CXCL12 and cell adhesion molecule VCAM-1 were increased, suggesting that depleting LNSC Lama5 promoted T cells entering the LNs by upregulating these migration-related molecules. Lymphocyte migration and enhanced chemokine production may function in a positive feedback loop so that enhanced lymphocyte flow driven by chemokines then stimulates stromal cells to produce more chemokines (50). DCs enhance stromal cell production of CCL21, which in turn facilitates lymphocyte migration (41). We also showed that while Lama5 enhanced T cell migration into the LNs, it did not regulate LN retention. Thus, adoptively transferred iTregs and naive CD4⁺ T cells were increased in Lama5-KO CR and HEVs (Figure 6A), yet blocking CD62L results in similar LN egress in WT and KO LNs (Supplemental Figure 12).

In considering the relatively increased abundance of Tregs in the Lama5-KO LNs, it is worth noting that both Tregs and naive CD4⁺ T cells express CCR7 (receptor for CCL21 and CCL19) and CXCR4 (CXCL12 receptor) (51). This is commensurate with our in vivo migration data showing no difference between naive CD4⁺ T cells and Tregs (Figure 5). However, Tregs have a different pattern of chemokine receptor expression compared with effector cells (e.g., TH1, TH2, TH17), which rarely express CCR7 and CXCR4 (51). Therefore, CCL19, CCL21, and CXCL12 may selectively drive

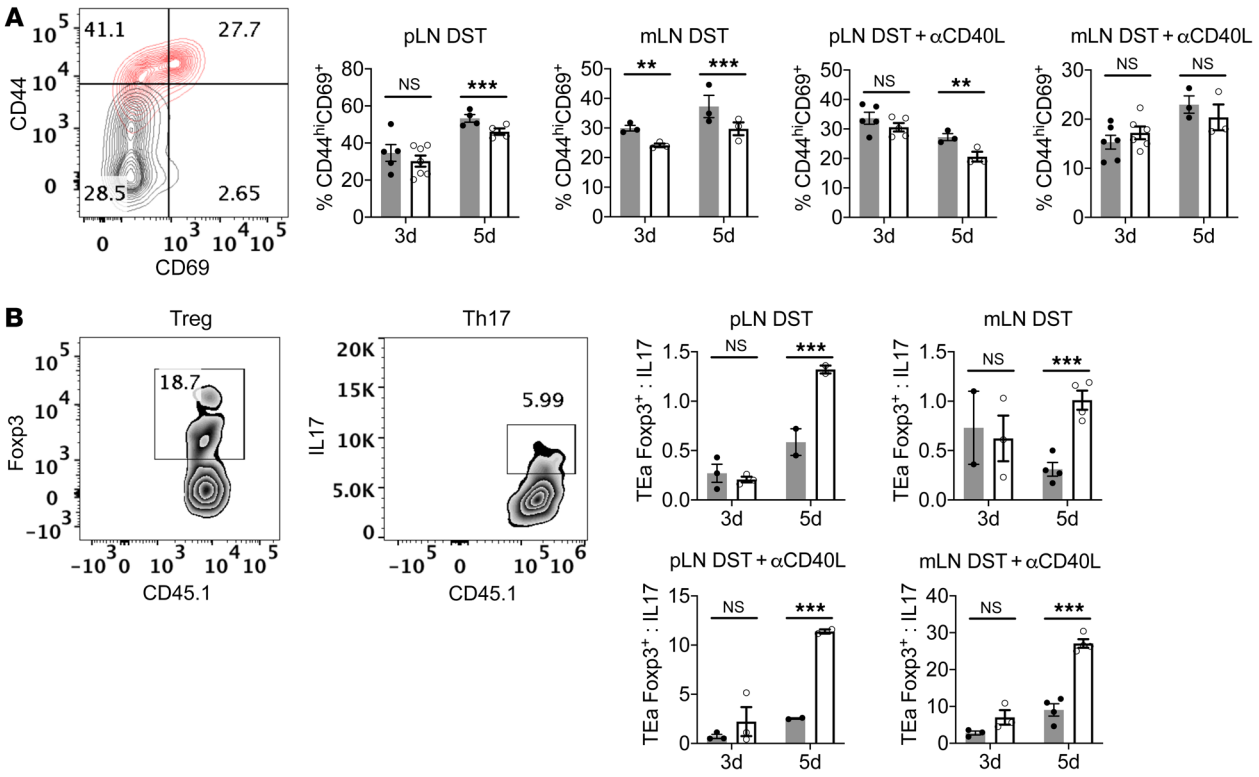

Figure 9. LN stromal Lama5 regulates antigen-specific CD4⁺ T cell responses in immunity and tolerance. CD45.1⁺CD4⁺ TEa cells (1×10^6) were injected i.v. into immune (plus 1×10^7 DST) or tolerant (plus 1×10^7 DST and 250 μg anti-CD40L) Lama5-KO and WT mice. WT mice only injected with TEa cells served as negative control (naive). (**A**) CD44 and CD69 expression on TEa cells 3 and 5 days after injection. Left graph: Gating strategy with WT pLNs; values show population percentage. Right panels: $CD44^{hi}CD69^{+}$ populations in pLNs and mLNs (n = 3–5). (**B**) TEa cell differentiation into Tregs or Th17 cells 3 and 5 days after injection. Left panels: Gating strategy with WT pLNs with DST plus anti-CD40L; values show population percentage. Right panels: Treg/Th17 ratios in SLOs under immunity and tolerance induction (n = 3). Data (mean ± SEM) are representative of 2 independent experiments. Gray bars, WT; white bars, KO. $^{**}P < 0.01$, $^{***}P < 0.001$ by unpaired, 2-tailed Student's t test.

naive T cells and Tregs into the LNs. As we previously showed (52), those naive T cells are driven to differentiate into Tregs in a tolerant environment. Furthermore, in the present study, we detected a difference in the retention of naive CD4⁺ T cells compared with Tregs in the cell egress assay. After blocking entry of cells into LNs using anti-CD62 mAb, both endogenous and adoptively transferred Tregs were retained in LNs compared with naive CD4⁺ T cells that exited the LNs (Supplemental Figure 12), leading to higher levels of Tregs in LNs.

Lymphocyte location in LN microdomains is associated with distinct cell fates. The CR contains a higher concentration of FRCs and is a site for T cell and DC interactions crucial for tolerance induction and maintenance (53). Th17 cells and Tregs are primed in the CR and the choice between immunity and tolerance may depend on other local factors, such as stromal laminin signals, as shown here (54). Induction of adaptive iTregs occurred preferentially in the CR compared with spleen (Figure 7C), consistent with the earlier report showing that iTreg induction occurs preferentially in LNs (55). CCL21 on HEVs serves as the major chemotactic force for recruiting plasmacytoid DCs from blood to trigger iTreg generation (30). In contrast, the spleen does not have HEV structures, again emphasizing the integral role of LNs in adaptive tolerance. The Treg/Th17 ratio was increased in Lama5-KO CR in both suppressed and immune conditions (Figures 7C and 9C). This accords well with our in vitro data showing that Lama5 promotes Th17 while suppressing Treg differentiation (56). Our findings also demonstrate that the laminin signals can be dominant regardless if the environment is proimmunogenic or proregulatory. With the addition of pharmacologic immunosuppressants, prolonged allograft acceptance was obtained by genetically depleting stromal Lama5 or blocking the T cell Lama5 receptors, indicating that suppressing Lama5 expression or function favors long-term immune regulation and suppression. In our previous study, a robust alloantibody response in the cardiac transplantation model was not observed (24), indicating that the enhanced cardiac graft survival due to deletion of Lama5 was mostly likely dependent on inhibition of cellular immunity. Further, the Lama5-KO mice and the anti–Lama5 receptor–treated mice appeared as healthy as the WT or untreated, and did not have cytokine storms or other types of pathologic responses, as assessed by the clinical condition of the animals, to account for the inhibition of immunity caused by interfering with Lama5 function or expression. These observations excluded other pathological or serological variables that accounted for changes in graft survival. The strategy of modulating tolerance through suppressing Lama5 may be translatable to humans with mAbs directed against Lama5, α6 integrin, or αDG.

This study, for the first time to our knowledge, demonstrated the in vivo role of LNSC Lama5, especially expressed by FRCs in immune

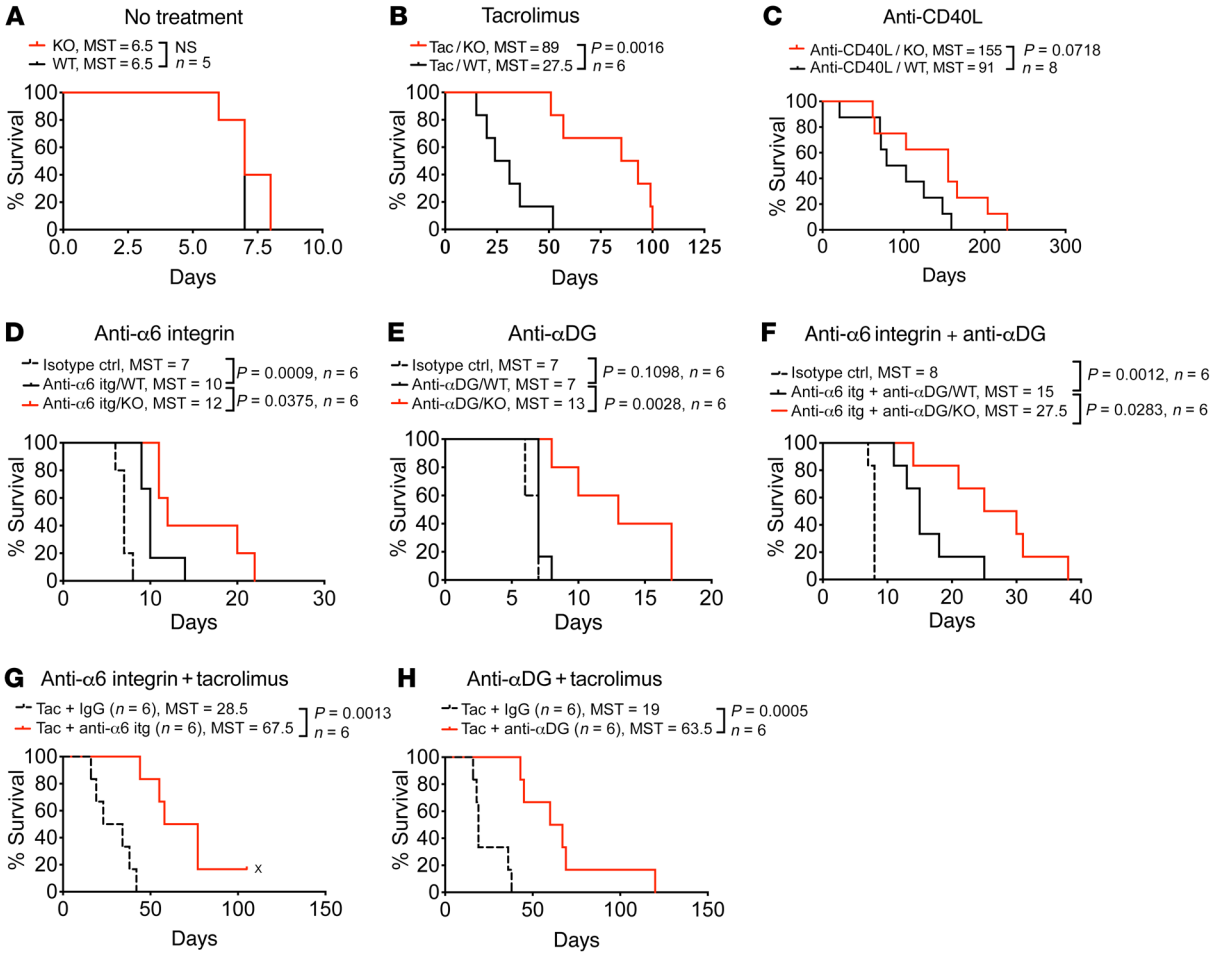

Figure 10. LN stromal Lama5 regulates alloimmunity. (**A**) Lama5-KO and WT mice received BALB/c cardiac allografts alone, (**B**) with tacrolimus (2 mg/kg/day s.c.), or (**C**) with anti-CD40L mAb (250 μg i.v. day 0). (**D**–**F**) Anti–α6 integrin mAb, anti-αDG mAb, or isotype controls (10 μg each i.v.) were administered every 3 days. (**G** and **H**) Anti–α6 integrin, anti-αDG mAb, or isotype control (10 μg i.v., every 7 days) with tacrolimus (2 mg/kg/day s.c.). Graft survival with log-rank comparisons; *n* = 6–8 mice/group. Median survival time (MST) was calculated. In **G**, the "x" indicates that the mouse died before rejection was observed. In **A**–**H**, *n* values indicate numbers of transplanted mice. $P < 0.05$ was considered statistically significant.

regulation. Lama5 depletion altered LN structure and chemokine and integrin regional expression, and thus promoted T cell migration into the LNs while simultaneously channeling T cell differentiation. Manipulating Lama5 expression or function created a suppressive niche in the LNs that promoted allograft acceptance, identifying an effective therapeutic target to modulate immunity. The LN scaffold components such as stromal collagens and other fibers, ER-TR7, cytokines, chemokines, and adhesion molecules comprise the LN microenvironment that regulate the behavior of trafficking T cells. Depleting Lama5 affected the expression of neighboring molecules on FRCs and other stromal cells and leukocytes. Further studies will be required to tease out additional molecular processes that underlie the changes in LN structure and function. For example, how laminins interact with the CD40-CD40L cascade and LTαβ-LTβR and NF-κB signaling pathways may be particularly revealing.

Methods

Mice. C57BL/6 (H-2^b) and BALB/c (H-2^d) mice were from The Jackson Laboratory. *Pdgfrb*-Cre$^{+/-}$ mice (29), a gift from Ralf Adams (Max Planck Institute for Molecular Biomedicine, Muenster, Germany), were crossed with *Lama5*-floxed mice (28), a gift from Jeff Miner (Washington University School of Medicine, St. Louis, Missouri, USA) and backcrossed with C57BL/6 for 10 generations. The Lama5 conditional KO mice (*Pdgfrb*-Cre$^{+/-}$ × *Lama5*$^{fl/fl}$) are healthy, fertile, and without abnormal findings when aging, such as colitis, alopecia, weight loss, or other signs of infection or autoimmunity. T cell receptor–transgenic mice expressing the TEa TCR (recognizing I-A^e antigen in the context of I-A^b) were acquired from A.Y. Rudensky (Memorial Sloan Kettering Cancer Center, New York, New York, USA). Experiments were conducted with age- and sex-matched mice at 8–12 weeks of age.

Reagents and antibodies. Laminin 411 and 511 were from Biolamina. CFSE and eFluor 670 were from Molecular Probes. Tacrolimus (USP grade) was from Sigma-Aldrich. IL-2 and TGF-β were from Invitrogen, and mouse and human CCL21 were from R&D Systems. The antibodies used in this study are shown in Supplemental Table 1.

Cell preparations. CD4$^+$ and CD8$^+$ T cells were isolated from LNs and spleens using the EasySep Mouse CD4 T cell isolation kit (catalog 19852, Stemcell Technologies) and EasySep Mouse CD8 T cell isolation kit (catalog 19853A, Stemcell Technologies), respectively. DCs and B cells were obtained through sorting CD11c$^+$ and B220$^+$

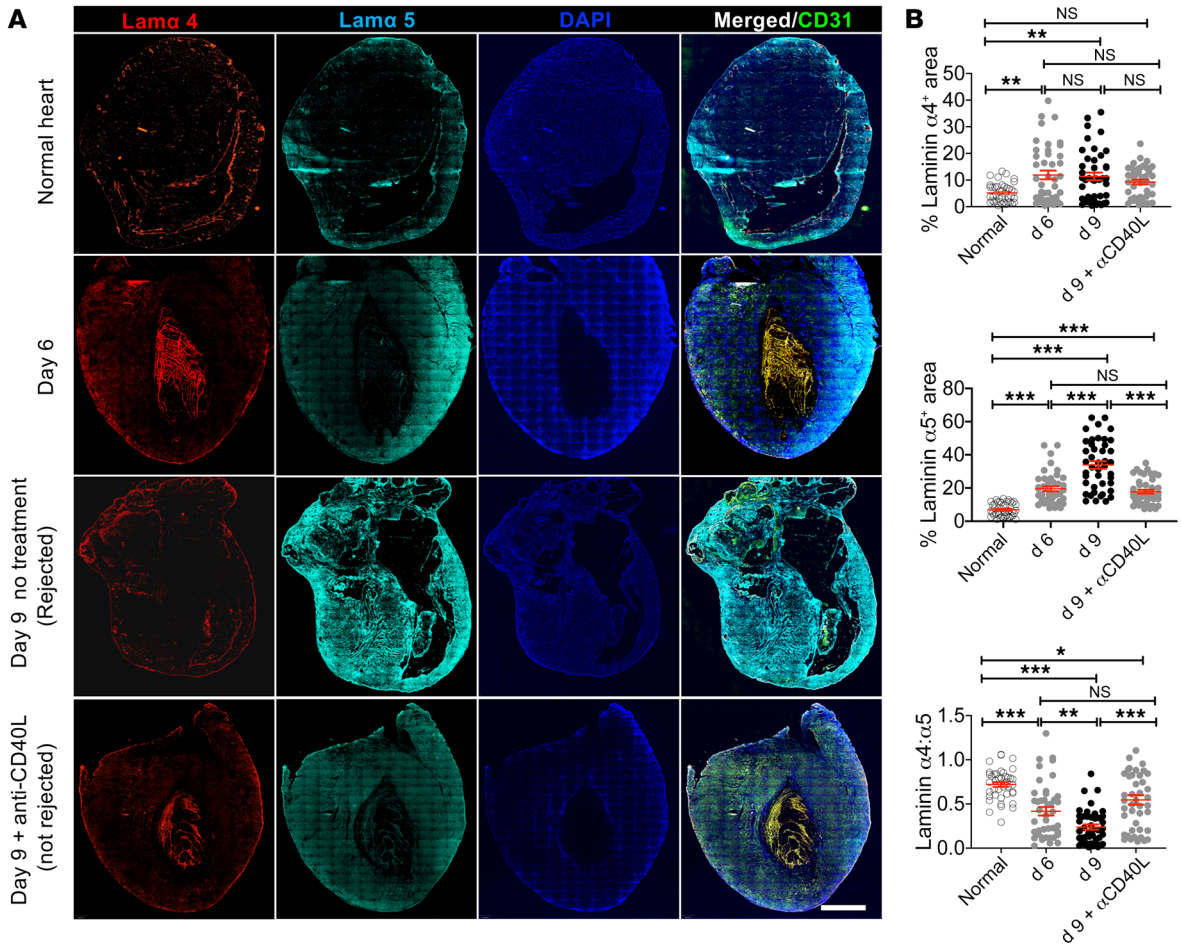

Figure 11. Lama4 and Lama5 in grafts are associated with rejection severity. Normal hearts, transplanted hearts on day 6 (not yet rejected) and day 9 (no treatment, rejected; anti-CD40L treated, not yet rejected) were stained for Lama4, Lama5, CD31, and with DAPI. (**A**) Representative whole-section images (original magnification, ×20). Scale bar: 800 μm. (**B**) Quantification of Lama4- and Lama5-positive areas and Lama5/Lama4 ratios (n = 45); DAPI-negative ventricular lumen omitted. Data (mean ± SEM) are representative of 3 independent experiments with 3 mice/group, 3 sections/graft. $^*P < 0.05$; $^{**}P < 0.01$; $^{***}P < 0.001$ by 1-way ANOVA with Tukey's multiple-comparisons test for multiple-variable differences.

cell populations, respectively. The splenocytes isolated from BALB/c mouse spleens were used for donor-specific transfusion. $CD4^+$ TEa cells were isolated from CD45.1-TEa TCR-transgenic mice using the mouse $CD4^+$ T cell isolation kit. nTregs ($CD4^+CD25^{hi}$) and memory $CD4^+$ T cells ($CD4^+CD44^{hi}$) from naive C57BL/6 mice were isolated with flow cytometry sorting. For iTregs, $CD4^+$ T cells isolated from Foxp3-GFP mice (5×10^4 cells per well) were cultured for 5 days in pro-Treg medium containing IL-2 (20 ng/mL, Thermo Fisher Scientific), anti-CD3ε mAb (1 mg/mL), anti-CD28 (1 mg/mL), and human TGF-β1 (10 ng/mL, Sino Biological). GFP^+ cell populations were sorted. FRCs ($CD31^-GP38^+$), BECs ($CD31^+GP38^-$), and LECs ($CD31^+GP38^+$) were sorted from the stromal cells harvested through enzymatic digestion of mouse LNs as described by Fletcher et al. (10).

Human Tregs were isolated from peripheral blood mononuclear cells using anti-CD25 microbeads (Miltenyi Biotec). The nTregs ($CD4^+CD25^{hi}CD127^-CD45RA^+$) and naive $CD4^+$ T cells ($CD4^+CD25^-CD127^+CD45RA^+$) were sorted. The purified nTregs were stimulated with irradiated KT64/86 cells cultured in XVivo-15 (BioWhittaker) media containing 10% human AB serum (Valley Biomedical), penicillin/streptomycin (Invitrogen), N-acetyl cysteine (USP), and recombinant IL-2 (300 IU/mL; Chiron) for 14 days. Before using, frozen nTregs and $CD4^+$ T cells were thawed and restimulated with anti-CD3/CD28 mAb-Dynabeads (Life Technologies) at 1:3 (cell/bead) plus recombinant IL-2 (300 U/mL) for 10 days before experiments (57).

Immunosuppression and tolerogenic regimens. For immunosuppression, mice were treated with 1 dose of anti-CD40L mAb (MR1, 0.25 mg i.v., BioXCell) or received daily tacrolimus (2 mg/kg/d s.c.). To block Lama5 receptors, anti–α6 integrin mAb (clone GoH3, BioLegend) or anti-αDG mAb (clone IIH6C4, Merck Millipore) was administered at 10 μg i.v. every 3 days. Tolerance and immunity were induced as previously described (44). Briefly, mice were tolerized i.v. with 1×10^7 donor splenocytes and 250 μg anti-CD40L mAb. Immune mice received DST only. $CD45.1^+CD4^+$ TEa cells (1×10^6) were adoptively transferred at the time of immunity or tolerance induction. Immunity and tolerance or suppression were assessed by measuring T cell responses including proliferation, activation ($CD44^{hi}CD69^+$), transcription factors (Foxp3), and cytokines (IL-17). $Foxp3^+$ Tregs and $IL\text{-}17^+$ Th17 cells were measured through flow cytometry to indicate tolerance and immunity, respectively. Data are presented as Treg/Th17 ratios to indicate the balance of tolerance versus immunity.

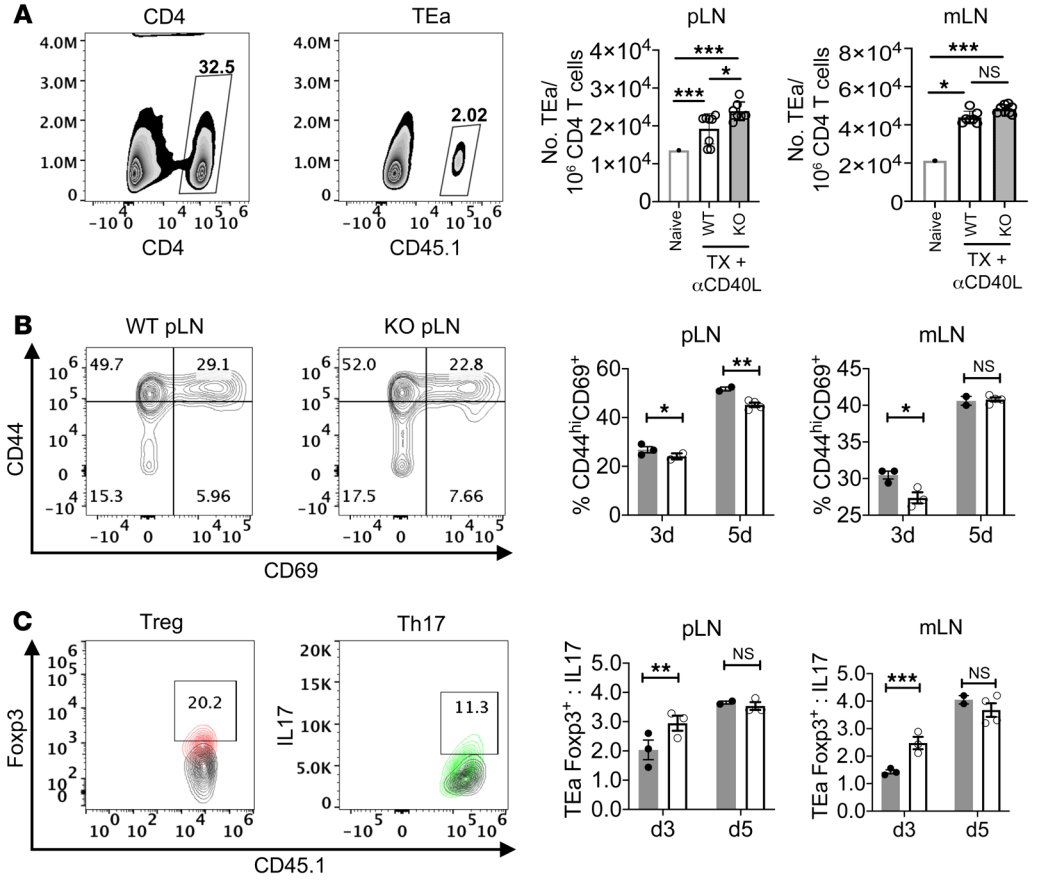

Figure 12. LN stromal Lama5 regulates graft-reactive cell responses. CD45.1$^+$CD4$^+$ TEa cells (1 × 10^6) and 250 μg anti-CD40L were injected i.v. into Lama5-KO and WT recipients on the day of BALB/c heart transplantation. WT mice only injected with TEa cells without transplantation served as negative controls (naive). LNs were harvested after 3 and 5 days. (**A**) Number of TEa cells out of 1 × 10^6 CD4$^+$ T cells 3 days after transplantation. Left panels: Gating strategy for CD4$^+$ T cells and TEa cells in WT pLNs (n = 6). (**B**) CD44 and CD69 expression by TEa cells at 3 and 5 days after transplantation. Left panels: Representative graphs with WT and Lama5-KO pLNs; values show population percentage (n = 3). (**C**) TEa cell differentiation into Tregs and Th17 cells 3 and 5 days after transplantation. Left panels: Gating strategy for Foxp3$^+$ and IL-17$^+$ TEa cells in WT pLNs; values indicate population percentage. Right panels: Treg/Th17 ratios (n = 3). Data (mean ± SEM) are representative of 2 independent experiments. White bars, WT; gray bars, KO. *P < 0.05; **P < 0.01; ***P < 0.001 by 1-way ANOVA with Tukey's multiple-comparisons test for multiple-variable differences (**A**) or unpaired, 2-tailed Student's t test for single-variable differences (**B** and **C**).

Cardiac allograft transplantation. Lama5-KO or WT mice (C57BL/6) were transplanted with heterotopic cardiac allograft from sex-matched donor BALB/c mice, as previously described (58). On the day of transplantation, mice were treated with anti-CD40L or received daily tacrolimus. To block Lama5 receptors, recipients were treated with anti–α6 integrin mAb or isotype control (rat IgG2a), or anti-αDG mAb or isotype control (IgM) every 3 or 7 days. Five to 8 mice per group were transplanted, as indicated by n values in Figure 10. Graft function was monitored daily by abdominal palpation until rejection.

Flow cytometry. Mouse LNs and spleen were passed through 70-μm nylon mesh screens (Thermo Fisher Scientific) to produce single-cell suspensions (59). Cell suspensions were treated with anti-CD16/32 (clone 93, eBioscience) to block Fc receptors, and then stained with antibodies against surface molecules and washed 2 times in FACS buffer (PBS with 0.5% w/v BSA). Flow cytometry antibody clones, fluorochromes, concentrations, vendors, and catalog numbers are listed in Supplemental Table 1. Samples were analyzed with an LSR Fortessa Cell Analyzer (BD Biosciences). Data were analyzed with FlowJo software version 10.6 (Tree Star).

Immunohistochemistry. LNs isolated from mice were excised and frozen in OCT (Sakura Finetek) on dry ice. The LN cryosections were cut in triplicate at 6 μm using a Microm HM 550 cryostat (Thermo Fisher Scientific). Sections attached on slides were fixed with cold acetone/ethanol (1:1) solution and washed in PBS buffer (Lonza). Primary antibodies and isotype controls are shown in Supplemental Table 1 and diluted according to the manufacturers' protocols and added to slides for 1 hour. Sections were washed with PBS, blocked with 5% monkey serum, and incubated with secondary antibodies for 90 minutes. Slides were then fixed wiath 4% paraformaldehyde (PFA)/PBS solution (Alfa Aesar) for 5 minutes. After washing slides in PBS for 15 minutes, the sections were incubated with 1% glycerol for 5 minutes. Prolong Gold Antifade Mountant with or without DAPI (Thermo Fisher Scientific) was added before covering the sections with cover slides. Images were acquired using an EVOS FL Auto 2 Imaging system and analyzed with Volocity image analysis software version 6.1.1 (PerkinElmer). The percentage positive staining area was quantified based on at least 3 independent experiments with 3 mice/group, 3 LNs/mouse, 3 sections/LN, and 3–5 fields/section.

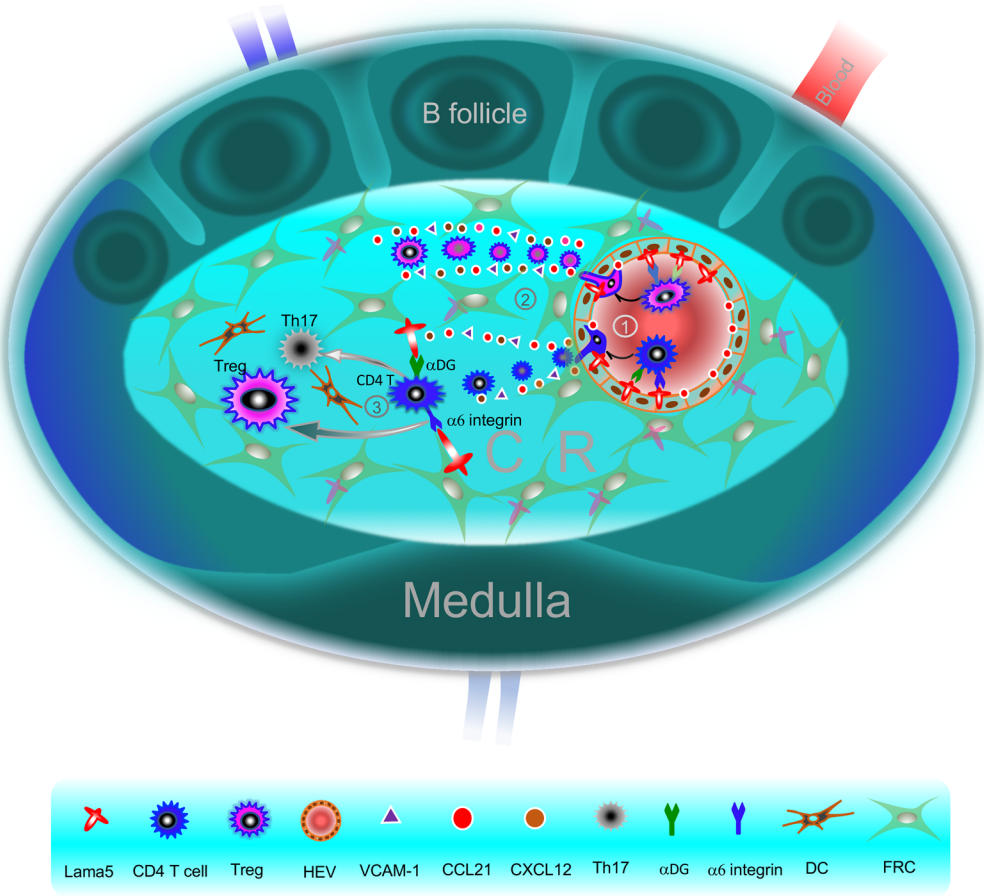

Figure 13. Schematic presentation of the role of Lama5 in T cell migration and CD4⁺ T cell differentiation in LNs. (1) Lama5 inhibits CD4⁺ T cell and Treg migration across HEVs to enter the LN cortical ridge through α6 integrin and αDG receptors on T cells. (2) Depleting Lama5 increases the number of HEVs and upregulates CCL21, CXCL12, and VCAM-1, which regulate T cell trafficking in the LN. (3) Lama5 promotes CD4⁺ T cell differentiation into Th17 cells and inhibits the differentiation into Tregs.

Real-time 2-dimensional imaging. CD4⁺ T cells were stained with a Cell Trace CFSE Cell Proliferation Kit (Thermo Fisher Scientific). CFSE⁺CD4⁺ T cells (5×10^5) were seeded into each well of a 24-well plate coated with laminin 411 (2 μg/mL) or laminin 511 (1 μg/mL). CD4⁺ T cell motility and migration were visualized with an EVOS FL Auto Imaging System (Life Technologies) with a 20× objective. One image was captured every 5 minutes for 2 hours. Distance from origin and velocity were analyzed with Volocity version 6.1.1.

Transmigration assay. Laminin 411 or 511 was diluted in 0.2% gelatin/DPBS to 30 μg/mL and coated onto 5-μm porous Transwell inserts set in a 24-well plate (Costar, Corning Inc.) at 37°C for 2 hours (8). Two to 3 days before the transmigration assay, MS-1 BECs (ATCC, CRL-2279) in 10% DMEM were seeded into the top of the laminin-coated Transwell insert and grown to confluence. CCL21 (0.5 μg/mL; R&D Systems) in 600 μL fresh 0.5% BSA media was added to the bottom well; 5×10^5 CFSE-labeled CD4⁺ T cells were added to the top of the insert, and the plate was incubated at 37°C in 5% CO_2 for 3 hours. Cells were quantified in the bottom wells to assess migration across inserts.

Cell perfusion assay. A BioFlux 1000 system (Fluxion Biosciences) coupled with an automated Axio Observer Z1 microscope (Carl Zeiss) was used to perform cell perfusion assays (8). CD4⁺ T cells were stained with a Cell Trace CFSE Cell Proliferation Kit (catalog C34554); 100 μL CFSE⁺ T cells (3.0×10^6 cells/mL) were perfused through channels under a shear-flow force of 0.5 dynes/cm² at 37°C.

Additionally, a multifunctional fluid flow device (34) that supplies turbulent shear flow over BECs was used. Briefly, each well of a 96-well plate was coated with 50 μL of 5 μg/mL fibronectin (Sigma-Aldrich) per well for 1 hour at 37°C, and then 50 μL of laminin 411 (30 μg/mL) or 511 (30 μg/mL) or both were incubated for 2 hours at 37°C. MS-1 cells (3×10^5) were then placed in each well and cultured 24 hours to obtain confluent monolayers, and then 100 μL CCL21 (0.5 μg/mL) was incubated in the wells for 6 hours. Ten milliliters of CFSE⁺ T cells (3.0×10^5 cells/mL) were perfused over the MS-1 monolayer with a syringe pump (Braintree Scientific, Inc.) at 3.5 mL/min (4 dynes/cm²). The number of CD4⁺ T cells attached to the endothelial cell monolayer was analyzed through quantifying the fluorescence images using ImageJ software version 1.5 (NIH). Four representative fields were imaged in each well, at least 4 wells for each condition, and the data were analyzed based on 3 independent experiments.

In vivo migration assay. In vivo blood migration assays were performed to evaluate T cell migration as previously published (60). Briefly, mice were injected i.v. with 2×10^6 eFluor 670-stained naive CD4⁺ T cells and 2×10^6 CFSE–stained iTregs, with staining protocols following the manufacturer's instructions. The mice were euthanized 16 hours after injection. LNs were harvested for cryosections and labeled T cell entry into LNs was analyzed through immunohistochemistry as described above.

qRT-PCR. Lama5 mRNA expression levels were quantified by qRT-PCR using the SYBR Green PCR kit (QIAGEN) and Applied Biosystems 7900HT Fast Real-time PCR System (Life Technologies). RNA isolation, reverse transcription, and PCR were conducted as described previously (59). Primer sequences were the following: Lama5, forward 5′-GGACCTCTACTGCAAGCTGGT-3′ and reverse 5′-ATAGGCCACATGGAACACCTG-3′; Lama4, forward 5′-AAGCCTCAAGAAAGG-

GTATGC-3′ and reverse 5′-AAATGTTGCCCTATGGCTTG-3′; CCL19, forward 5′-ATGCGGAAGACTGCTGCC-3′ and reverse 5′-CGGAAGGCTTTCACGATGTT-3′; CCL21, forward 5′-TCCCGGCAATCCTGTTCTT-3′ and reverse 5′-CCTTCCTCAGGGTTTGCACA-3′; CXCL12, forward 5′-CTCTGCATCAGTGACGGTAA-3′ and reverse 5′-CTTCAGCCGTGCAACAATCT-3′; VCAM-1, forward 5′-GCAGGATGCCGGCATATACG-3′ and reverse 5′-TGCGCAGTAGAGTGCAAGGA-3′; ICAM-1, forward 5′-CACCCCAAGGACCCCAAGGAGAT-3′ and reverse 5′-CGACGCCGCTCAGAAGAACCA-3′; MAdCAM-1, forward 5′-AGAAGAGGAGATACAAGAGG-3′ and reverse 5′-TAGTGTCTGGGCGAGGACC-3′; VEGF-A, forward 5′-TTACTGCTGTACCTCCACC-3′ and reverse 5′-ACAGGACGGCTTGAAGATG-3′; VEGF-C, forward 5′-ACCGTGTGCGAATCGACTG-3′ and reverse 5′-AATACGATGGGACACAGCGG-3′; VEGF-D, forward 5′-TTGACCTAGTGTCATGGTAAAGC-3′ and reverse 5′-TCAGTGAACTGGGGAATCAC-3′; Cyclophilin A, forward 5′-AGGGTGGTGACTTTACACGC-3′ and reverse 5′-ATCCAGCCATTCAGTCTTGG-3′; αDG, forward 5′-CTGGAAGAACCAGCTTGAGG-3′ and reverse 5′-ATGACTGTGTGGGTCCCAGT-3′. PCR consisted of a 15-minute 95°C denaturation step followed by 45 cycles of 15 seconds at 94°C, 20 seconds at 56°C, and 20 seconds at 72°C. Normalized values for specific gene expression were calculated as using $2^{-\Delta\Delta Ct}$. Each RNA sample was run in triplicate, and each experimental group consisted of 3 individual samples.

Statistics. All in vitro experiments were conducted at least 3 times individually with triplicate samples. In vivo migration experiments (3 mice/group) were performed at least 2 times. All transplantation experiments were performed 3 times. Immunohistochemistry was performed at least 3 times, 3 mice per group, and at least 3 LNs were collected from each mouse, 3 sections/LN, and over 5 fields/section were acquired. Fluorescence images were analyzed using Velocity software 6.1.1 for fluorescence density quantification and cell counting. Figures were organized using GraphPad Prism Software (version 8) and are presented as the mean ± SEM. Statistical analyses were performed using Student's *t* test for single-variable differences or 1-way ANOVA with Tukey's multiple-comparisons test for multiple comparisons. Statistical analysis of graft survival data was assessed by log-rank (Mantel-Cox) test. *P* less than 0.05 was considered statistically significant.

Study approval. All animal experiments were performed in accordance with protocols approved by the University of Maryland School of Medicine Institutional Animal Care and Use Committee (IACUC).

Author contributions

JSB and LL conceived the study, designed experiments, interpreted the data, and wrote the manuscript. LL, MWS, TZ, YX, WP, VS, CP, YL, NT, BMC, QL, TS, KDS, KLH, and BRB performed experiments. RA revised the manuscript and supplied constructive suggestions for interpreting results.

Acknowledgments

This study was supported by NIH grants 1R01AI114496 and R01AI062765 (to JSB), R6029–07 (to BRB), R01 HL11879, P01 AI056299 (to BRB), and NCI P01 CA067493 (to BRB). We thank Ralf Adams and Lijun Xia for providing Pdgfrb-Cre mice, and Jeffrey H. Miner for supplying Lama5-floxed ($CLA5^{fl/fl}$) mice. We appreciate Katrina M. Williams and Joseph P. Stains for their help with cell flow assays. We appreciate the flow cytometry sorting work performed by the University of Maryland Marlene and Stewart Greenebaum Cancer Center Flow Cytometry Shared Service.

Address correspondence to: Jonathan S. Bromberg, Department of Surgery and Microbiology and Immunology, University of Maryland School of Medicine, 22 S. Greene Street, S8B06 Baltimore, Maryland 21201, USA. Phone: 410.328.6430; Email: jbromberg@som.umaryland.edu.

1. Bajénoff M, et al. Stromal cell networks regulate lymphocyte entry, migration, and territoriality in lymph nodes. *Immunity*. 2006;25(6):989–1001.
2. Perez-Shibayama C, Gil-Cruz C, Ludewig B. Fibroblastic reticular cells at the nexus of innate and adaptive immune responses. *Immunol Rev*. 2019;289(1):31–41.
3. Gretz JE, Anderson AO, Shaw S. Cords, channels, corridors and conduits: critical architectural elements facilitating cell interactions in the lymph node cortex. *Immunol Rev*. 1997;156:11–24.
4. Malhotra D, et al. Transcriptional profiling of stroma from inflamed and resting lymph nodes defines immunological hallmarks. *Nat Immunol*. 2012;13(5):499.
5. Nakayama Y, Bromberg JS. Lymphotoxin-beta receptor blockade induces inflammation and fibrosis in tolerized cardiac allografts. *Am J Transplant*. 2012;12(9):2322–2334.
6. Kumar V, et al. A dendritic-cell-stromal axis maintains immune responses in lymph nodes. *Immunity*. 2015;42(4):719–730.
7. Willard-Mack CL. Normal structure, function, and histology of lymph nodes. *Toxicol Pathol*. 2006;34(5):409–424.
8. Warren KJ, Iwami D, Harris DG, Bromberg JS, Burrell BE. Laminins affect T cell trafficking and allograft fate. *J Clin Invest*. 2014;124(5):2204–2218.
9. Ruddle NH. High endothelial venules and lymphatic vessels in tertiary lymphoid organs: characteristics, functions, and regulation. *Front Immunol*. 2016;7:491.
10. Fletcher AL, et al. Reproducible isolation of lymph node stromal cells reveals site-dependent differences in fibroblastic reticular cells. *Front Immunol*. 2011;2:35.
11. Brown FD, Turley SJ. Fibroblastic reticular cells: organization and regulation of the T lymphocyte life cycle. *J Immunol*. 2015;194(4):1389–1394.
12. Gretz JE, Norbury CC, Anderson AO, Proudfoot AE, Shaw S. Lymph-borne chemokines and other low molecular weight molecules reach high endothelial venules via specialized conduits while a functional barrier limits access to the lymphocyte microenvironments in lymph node cortex. *J Exp Med*. 2000;192(10):1425–1440.
13. Sixt M, et al. The conduit system transports soluble antigens from the afferent lymph to resident dendritic cells in the T cell area of the lymph node. *Immunity*. 2005;22(1):19–29.
14. Chai Q, et al. Maturation of lymph node fibroblastic reticular cells from myofibroblastic precursors is critical for antiviral immunity. *Immunity*. 2013;38(5):1013–1024.
15. Link A, et al. Fibroblastic reticular cells in lymph nodes regulate the homeostasis of naive T cells. *Nat Immunol*. 2007;8(11):1255–1265.
16. Brown FD, Turley SJ. Fibroblastic reticular cells: organization and regulation of the T lymphocyte life cycle. *J Immunol*. 2015;194(4):1389–1394.
17. Rodda LB, et al. Single-cell RNA sequencing of lymph node stromal cells reveals niche-associated heterogeneity. *Immunity*. 2018;48(5):1014–1028.e6.
18. Sanchez JL, et al. Lymphoid fibrosis occurs in long-term nonprogressors and persists with antiretroviral therapy but may be reversible with curative interventions. *J Infect Dis*. 2015;211(7):1068–1075.
19. Knoblich K, et al. The human lymph node microenvironment unilaterally regulates T-cell activation and differentiation. *PLoS Biol*. 2018;16(9):e2005046.
20. Lee HJ, et al. The micronucleus frequency in cytokinesis-blocked lymphocytes of cattle in the vicinity of a nuclear power plant. *J Vet Sci*. 2007;8(2):117–120.
21. Cohen JN, et al. Lymph node-resident lymphatic endothelial cells mediate peripheral tolerance via Aire-independent direct antigen presentation. *J Exp Med*. 2010;207(4):681–688.
22. Malhotra D, et al. Transcriptional profiling of stroma from inflamed and resting lymph nodes defines immunological hallmarks. *Nat Immunol*.

2012;13(5):499–510.
23. Song J, et al. Extracellular matrix of secondary lymphoid organs impacts on B-cell fate and survival. *Proc Natl Acad Sci U S A*. 2013;110(31):E2915–E2924.
24. Bromberg JS, et al. Gut microbiota-dependent modulation of innate immunity and lymph node remodeling affects cardiac allograft outcomes. *JCI Insight*. 2018;3(19):121045.
25. Amin K, Janson C, Sevéus L, Miyazaki K, Virtanen I, Venge P. Uncoordinated production of Laminin-5 chains in airways epithelium of allergic asthmatics. *Respir Res*. 2005;6:110.
26. Spenlé C, et al. The laminin response in inflammatory bowel disease: protection or malignancy? *PLoS One*. 2014;9(10):e111336.
27. Gorfu G, et al. Laminin isoforms of lymph nodes and predominant role of alpha5-laminin(s) in adhesion and migration of blood lymphocytes. *J Leukoc Biol*. 2008;84(3):701–712.
28. Miner JH, Cunningham J, Sanes JR. Roles for laminin in embryogenesis: exencephaly, syndactyly, and placentopathy in mice lacking the laminin alpha5 chain. *J Cell Biol*. 1998;143(6):1713–1723.
29. Herzog BH, et al. Podoplanin maintains high endothelial venule integrity by interacting with platelet CLEC-2. *Nature*. 2013;502(7469):105–109.
30. Ochando JC, et al. Alloantigen-presenting plasmacytoid dendritic cells mediate tolerance to vascularized grafts. *Nat Immunol*. 2006;7(6):652–662.
31. Chyou S, et al. Fibroblast-type reticular stromal cells regulate the lymph node vasculature. *J Immunol*. 2008;181(6):3887–3896.
32. Xiong Y, et al. CD4 T cell sphingosine 1-phosphate receptor (S1PR)1 and S1PR4 and endothelial S1PR2 regulate afferent lymphatic migration. *Sci Immunol*. 2019;4(33):eaav1263.
33. Qian H, Tryggvason K, Jacobsen SE, Ekblom M. Contribution of alpha6 integrins to hematopoietic stem and progenitor cell homing to bone marrow and collaboration with alpha4 integrins. *Blood*. 2006;107(9):3503–3510.
34. Lyons JS, Iyer SR, Lovering RM, Ward CW, Stains JP. Novel multi-functional fluid flow device for studying cellular mechanotransduction. *J Biomech*. 2016;49(16):4173–4179.
35. Grubin CE, Kovats S, deRoos P, Rudensky AY. Deficient positive selection of CD4 T cells in mice displaying altered repertoires of MHC class II-bound self-peptides. *Immunity*. 1997;7(2):197–208.
36. Simon T, Bromberg JS. Regulation of the immune system by laminins. *Trends Immunol*. 2017;38(11):858–871.
37. Cupedo T, Mebius RE. Cellular interactions in lymph node development. *J Immunol*. 2005;174(1):21–25.
38. Vondenhoff MF, et al. LTbetaR signaling induces cytokine expression and up-regulates lymphangiogenic factors in lymph node anlagen. *J Immunol*. 2009;182(9):5439–5445.
39. Ager A. High endothelial venules and other blood vessels: critical regulators of lymphoid organ development and function. *Front Immunol*. 2017;8:45.
40. Moussion C, Girard JP. Dendritic cells control lymphocyte entry to lymph nodes through high endothelial venules. *Nature*. 2011;479(7374):542–546.
41. Wendland M, et al. Lymph node T cell homeostasis relies on steady state homing of dendritic cells. *Immunity*. 2011;35(6):945–957.
42. Onder L, et al. Endothelial cell-specific lymphotoxin-β receptor signaling is critical for lymph node and high endothelial venule formation. *J Exp Med*. 2013;210(3):465–473.
43. Webster B, Ekland EH, Agle LM, Chyou S, Ruggieri R, Lu TT. Regulation of lymph node vascular growth by dendritic cells. *J Exp Med*. 2006;203(8):1903–1913.
44. Burrell BE, Warren KJ, Nakayama Y, Iwami D, Brinkman CC, Bromberg JS. Lymph node stromal fiber ER-TR7 modulates $CD4^+$ T cell lymph node trafficking and transplant tolerance. *Transplantation*. 2015;99(6):1119–1125.
45. Förster R, Davalos-Misslitz AC, Rot A. CCR7 and its ligands: balancing immunity and tolerance. *Nat Rev Immunol*. 2008;8(5):362–371.
46. Ueha S, et al. CCR7 mediates the migration of $Foxp3^+$ regulatory T cells to the paracortical areas of peripheral lymph nodes through high endothelial venules. *J Leukoc Biol*. 2007;82(5):1230–1238.
47. Schulz O, Hammerschmidt SI, Moschovakis GL, Förster R. Chemokines and chemokine receptors in lymphoid tissue dynamics. *Annu Rev Immunol*. 2016;34:203–242.
48. Girard JP, Moussion C, Förster R. HEVs, lymphatics and homeostatic immune cell trafficking in lymph nodes. *Nat Rev Immunol*. 2012;12(11):762–773.
49. Bao X, et al. Endothelial heparan sulfate controls chemokine presentation in recruitment of lymphocytes and dendritic cells to lymph nodes. *Immunity*. 2010;33(5):817–829.
50. Tomei AA, Siegert S, Britschgi MR, Luther SA, Swartz MA. Fluid flow regulates stromal cell organization and CCL21 expression in a tissue-engineered lymph node microenvironment. *J Immunol*. 2009;183(7):4273–4283.
51. Bromley SK, Mempel TR, Luster AD. Orchestrating the orchestrators: chemokines in control of T cell traffic. *Nat Immunol*. 2008;9(9):970–980.
52. Burrell BE, Bromberg JS. Fates of $CD4^+$ T cells in a tolerant environment depend on timing and place of antigen exposure. *Am J Transplant*. 2012;12(3):576–589.
53. Katakai T, Hara T, Lee JH, Gonda H, Sugai M, Shimizu A. A novel reticular stromal structure in lymph node cortex: an immuno-platform for interactions among dendritic cells, T cells and B cells. *Int Immunol*. 2004;16(8):1133–1142.
54. Brinkman CC, et al. Anatomy of tolerance. *Curr Opin Organ Transplant*. 2013;18(4):393–401.
55. Bai Y, et al. L-selectin-dependent lymphoid occupancy is required to induce alloantigen-specific tolerance. *J Immunol*. 2002;168(4):1579–1589.
56. Simon T, et al. Differential regulation of T-cell immunity and tolerance by stromal laminin expressed in the lymph node. *Transplantation*. 2019;103(10):2075–2089.
57. Hippen KL, et al. Massive ex vivo expansion of human natural regulatory T cells (T(regs)) with minimal loss of in vivo functional activity. *Sci Transl Med*. 2011;3(83):83ra41.
58. Corry RJ, Winn HJ, Russell PS. Primarily vascularized allografts of hearts in mice. The role of H-2D, H-2K, and non-H-2 antigens in rejection. *Transplantation*. 1973;16(4):343–350.
59. Brinkman CC, et al. Treg enagage lymphotoxin beta receptor for afferent lymphatic transendothelial migration. *Nat Commun*. 2016;7:12021.
60. Piao W, et al. Regulation of T cell afferent lymphatic migration by targeting LTβR-mediated non-classical NFκB signaling. *Nat Commun*. 2018;9(1):3020.